RWTH Aachen University
Institute of Aerospace Systems

NASA/DLR Design Challenge 2019

aDEPt

Aircraft Design Concept

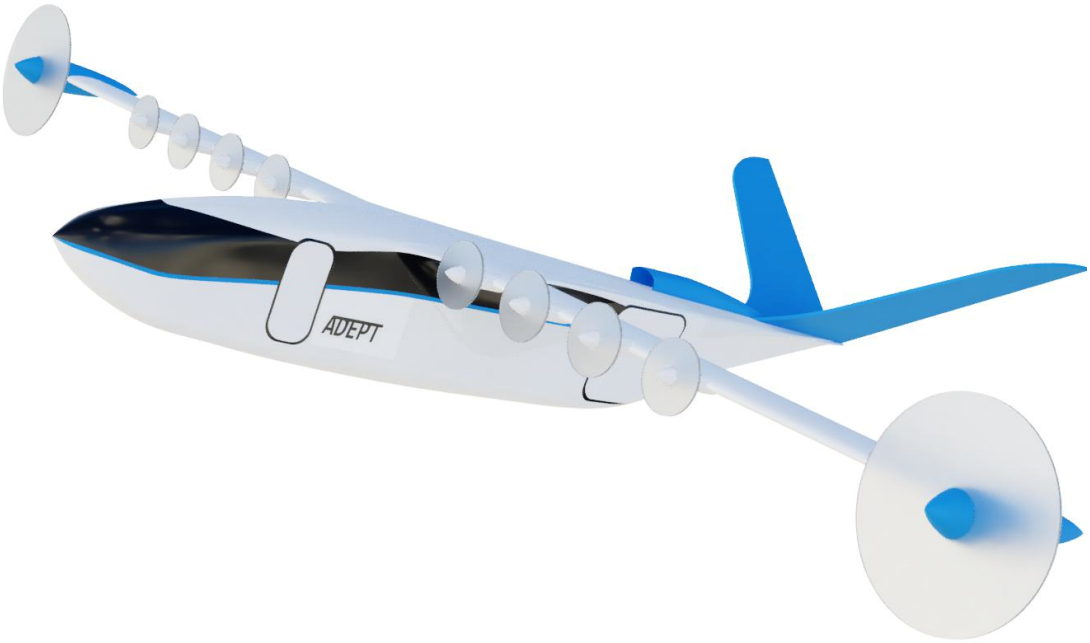

Team Members:

Kevin Poch, B.Sc. (Team Lead)
Arthur Graf
Fabian Breer
Joshuah Belflower, B.Sc.
Maximilian Bayer
Nicolas Schneiders, B.Sc.
Lukas Hennies (Team Lead)
Colin Klein
Jan Spittel
Marco Föry
Moritz vom Schemm
Steffen Tarner, B.Sc.

Academic Advisors:

Miguel Yael Pereda Albarrán, M.Sc.
Univ.-Prof. Dr.-Ing. Eike Stumpf

This project is submitted on July 1, 2019

Institut für Luft- und Raumfahrtsysteme, Wüllnerstr. 7, 52062 Aachen

INSTITUT FÜR LUFT- UND RAUMFAHRTSYSTEME

Univ.-Prof. Dr.-Ing. Eike Stumpf

Rheinisch-Westfälische
Technische Hochschule Aachen

Wüllnerstraße 7
52062 Aachen

Telefon 0241-80 968 01
Telefax 0241-80 922 33
sekretariat@ilr.rwth-aachen.de

www.ilr.rwth-aachen.de

Aachen, 27.06.2019

Attestation for Submission

The hereby submitted project work has been confirmed by the Head of Institute of Aerospace Systems (ILR) and is endorsed for the submission in the NASA/DLR Design Challenge 2019. The work has been done independently form currently enrolled students from RWTH Aachen University without further assistance of our institute.

Univ.-Prof. Dr.-Ing. Eike Stumpf

Mr. Miguel Yael Pereda Albarrán

Team Members

	Surname	Name	Field of study	Semester
		Back row (left to right)		
1	Spittel	Jan	Mechanical Engineering, B.Sc.	10
2	Breer	Fabian	Mechanical Engineering, B.Sc.	6
3	Belflower	Joshuah	Aerospace Engineering, M.Sc.	2
4	Tarner	Steffen	Aerospace Engineering, M.Sc.	2
5	Hennies	Lukas	Mechanical Engineering, B.Sc.	10
		Front row (left to right)		
6	Graf	Arthur	Mechanical Engineering, B.Sc.	6
7	Klein	Colin	Mechanical Engineering, B.Sc.	6
8	Schneiders	Nicolas	Aerospace Engineering, M.Sc.	2
9	Poch	Kevin	Aerospace Engineering, M.Sc.	1
10	Föry	Marco	Mechanical Engineering, B.Sc.	8
11	Bayer	Maximilian	Mechanical Engineering, B.Sc.	6
12	vom Schemm	Moritz	Mechanical Engineering, B.Sc.	8

Abstract

The *Aachen Distributed Electric Propulsion Transporter* (*aDEPt*) presents a versatile aircraft concept that offers an efficient and cost-effective transport model for connecting remote towns or small cities to larger central hubs in metropolitan areas. Key design features derived from requirements set by the current market demands include a hybrid-electric powertrain, distributed electric propulsion systems, a sensible cabin conversion and loading concept, a morphing trailing edge and an unpressurized cabin. Further constraints set by the NASA/DLR Design Challenge are met or exceeded by the *aDEPt* concept. The aircraft excels in terms of life cycle costs through optimized operation models, low noise emissions and high efficiency through the given propulsion system when compared to other thin-haul aircraft. Initial calculations, without autonomous flight, show that the *aDEPt* is 31.2%, 33.3% and 53.3% cheaper to operate than the P2012, C402, and PC12, respectively. This is, in part, due to the *aDEPt*'s capability of flying a fully electric 125 NM mission, which significantly reduces operating costs and emissions. The concept is designed for a maximum range of 350 NM with a cruise speed of 250 knots. Additionally the *aDEPt*'s avionics configuration allows for autonomous operations, making it a sustainable aircraft design for the coming years of aircraft operations without increasing design, development or production costs. The *aDEPt* is an aircraft design focused on cost reduction and flexibility using technology whose readiness level by 2025 is given the current state of the art and industry estimates for technological development.

Contents

List of Figures

List of Tables

Nomenclature

Abbreviations

5G	Fifth generation cellular network technology	18
AC	Alternating Current	6
ADS-B	Automatic Dependent Surveillance - Broadcast	18
AES	Advanced Encryption Standard	19
APU	Auxiliary Power Unit	7
ASM	Available Seat Mile	23
AUTO-GCAS	Automatic Ground Collision Avoidance System	18
BEP	Break Even Point	22
C402	Cessna 402 airplane	III
CA	Cape Air	1
CFD	Computational Fluid Dynamics	12
CFR	Code of Federal Regulations	2
CG	Center of Gravity	12
CP	Cruise Propeller	5
CPI	Consumer Price Index	21
DC	Disposal Costs	21
DDC	Design and Development Costs	21
DHL	DHL International GmbH	10
DLR	Deutsche Zentrum fuer Luft- und Raumfahrt	III
EAS	Essential Air Service	1

EGNOS	European Geostationary Navigation Overlay Service	18
EPAL1	Pallets with a dimension of 800 mm x 1 200 mm x 144 mm	10
EPAL2	Pallets with a dimension of 1000 mm x 1 200 mm x 162 mm	10
FAR	Federal Aviation Regulations	13
FLOPS	Flight Optimization System	13
FOC	Fixed Operating Costs	22
GAW-1	NASA/LANGLEY LS(1)-0417 (GA(W)-1) Airfoil	11
GAW-2	NASA/LANGLEY LS(1)-0413 (GA(W)-2) Airfoil	11
GMA	Pallets with a dimension of 40 x 48"	10
GP	Ground Pilot	19
GPS	Global Positioning System	18
GPU	Ground Power Unit	7
HLP	High Lift Propeller	5
HUD	Head-Up Display	18
IFR	Instrument Flight Rules	17
ILS	Instrument Landing System	18
IMC	Instrument Meteorological Conditions	17
IR	Infrared Radiation	18
ISC	Fraunhofer Institute for Silicate Research	15
KIAS	Indicated Airspeed in knots	3
LCC	Life Cycle Costs	21
LP	List Price	22
MAC	Mean Aerodynamic Chord	12
MEW	Manufacturer's Empty Weight	13
MTOW	Maximum Take Off Weight	5
NASA	National Aeronautics and Space Administration	III
NPV	Net Present Value	22

OC	Operating Costs	2
OpCo	Operating Concepts	19
P2012	Tecnam P2012 Traveller airplane	III
PAX	Number of Passengers	14
PC	Production Costs	21
PC12	Pilatus PC-12 airplane	III
PR	Production Rate	22
PSFC	Power Specific Fuel Consumption	8
PT6A-41	Gas Turbine	8
SATS	Small Aircraft Transportation System	15
SPL	Sound Pressure Level	16
STOL	Short T/O and Landing	19
T/O	Take-Off	5
TE	Trailing Edge	10
TFR	Terrain Following Radar	18
TG	Turbo Generator	4
TRL	Technology Readiness Levels	14
USD	US-Dollar	23
VOC	Variable Operating Costs	22
WAAS	Wide Area Augmentation System	18

Symbols

β_{eff}	Effective sliding angle at vertical tailplane	13
η_{AC}	AC engine efficiency	6
η_A	Power line efficiency	6
η_B	Battery efficiency	6
η_C	Controller efficiency	6

η_{GEN}	Generator efficiency	6
η_{GT}	Turbine efficiency	6
η_H	Ratio of the dynamic pressure at the horizontal tailplane	12
η_{INV}	Inverter efficiency	6
η_P	Propeller efficiency	6
η_{RC}	Rectifier efficiency	6
η_S	Ratio of the dynamic pressure at the vertical tailplane	13
ν	Angle of tailplane page to the horizontal	13
C_D	Drag coefficient	10
$C_{L,max}$	Maximum lift coefficient	5
C_{LH}	Lift coefficient of horizontal tail	12
C_L	Lift coefficient	5
$C_{m0FR,max}$	Coefficient: Torque of fuselage and wing	12
$C_{n\beta}$	Coefficient: Yaw rate caused by sliding angle	13
C_T	Thrust coefficient	12
$C_{Y\beta,S}$	Coefficient: Force in y-direction caused by sliding angle	13
K	Efficacy factors	13
OC_{DP}	Depreciation costs	24
r_H	Distance between pressure point of horizontal tail to CG	12
S_H	Horizontal tailplane area	12
S_S	Vertical tailplane area	13
S_V	V-Tail area	13
t_{OP}	Operating period	24
V_S	Stall Speed	13
V_T	Engine factor	12
x_{CGV}	Fordest point of gravity	12
x_N	Neutral point	12

x_S	Position pressure point vertical tailplane	13
y_t	Lever arm to failed engine	13
ΔT	Difference in thrust caused by engine failure	13
D	Drag force	5
i	Interest Rate	22
KTAS	True Air Speed in knots	5
L	Lifting frorce	5
LE	Leading Edge	10
M	Mach number	12
NM	Nautical Miles	III
Re	Reynolds number	12
S	Wing area	5
T	Time span in years	22
W	Weight force	5

1 Introduction and Market Analysis

Metropolitan areas of the world are commonly characterized as hubs of intermodal transport and by a strong economy. While the total world population living in metropolitan areas has superceded 50% as of 2007, a significant portion of the world population still lives in remote regions with limited access to various means of transport [27, 53, 54]. In this context, air transportation becomes more important for the trade of commercial goods, human mobility and economic development [55].

Airlines such as *Cape Air* (CA), America's largest commuter airline, are the vital link for rural communities to connect to larger hubs. In 2016, however, about half of CA's missions were subsidized by the *Essential Air Service* (EAS) program, as otherwise they would not be economically feasible [59].

This is rooted in the economic challenges of thin-haul air travel. The connection of remote regions to the next airport is characterised by short and inconsistently frequented routes, which make scheduled air service more difficult and increase *Operating Costs* (OC) disproportionately. For example, none of CA's routes exceeds 225 NM, two thirds of the flown routes are even shorter than 100 NM (see Figure 1.1) [59]. Nevertheless, CA's business model of non-stop, low-fare service in smaller aircraft consistently attracts more passengers, which underlines the increasing demand in this segment of air travel [60].

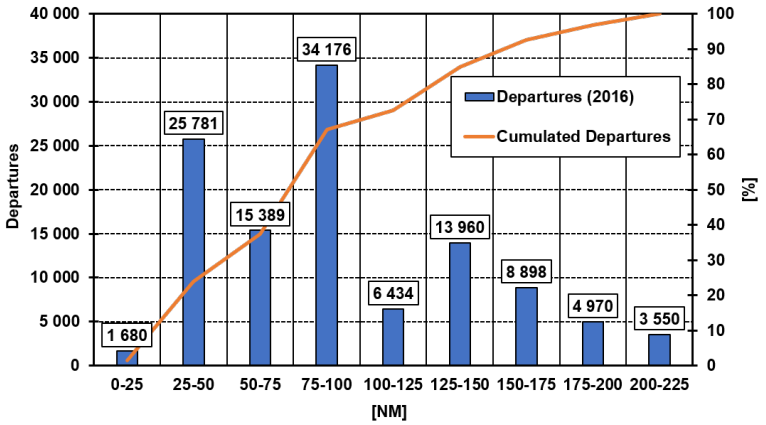

Figure 1.1: Route distribution of CA in 2016 based on [59]

However, none of the currently available 9-seater aircraft, like the widely used Pilatus PC-12 and Cessna 402 are optimized for the thin-haul market, which is especially evident in their excessive range capabilities. Additionally, many rural communities can be found in ecologically challenging areas that place additional demands on an aircraft like operating on water, under icing conditions or from very short and not paved runways. Due to the nature of this routes CA and other commuter airlines insist on operating multi-engine aircraft in the future to decrease error-proneness [60].

In addition to non-optimized aircraft, the burgeoning shortage of qualified pilots also prevents airlines like CA from growing further into the market and thus from integrating more communities into the air traffic network [60]. One way to avoid this problem is an increasingly autonomous air traffic. In a first

step, this can be achieved by increasing single pilot operation through human-centered automation. Fully autonomous, ground-monitored flights subsequently offer great potential for reducing OC and error-proneness. To further promote autonomy and reduce OC utilization can be increased through additional cargo transport outside the peak hours of passenger transport. This, however, places additional requirements on an aircraft, since an efficient cargo operation requires a sensible conversion and loading concept.

2 Design Selection

The configuration selection is conducted by taking into consideration the requirements given by the market and NASA/DLR. Figure 2.1 shows the overall schematic procedure conducted in this work.

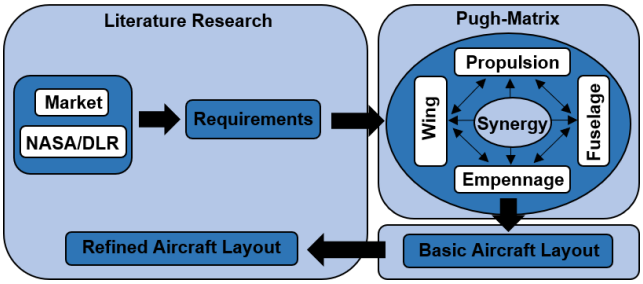

Figure 2.1: Methodology of the selection process

2.1 Basic Considerations

The best appropriate figures of merit must first be derived in order to determine a feasible concept that meets all requirements. The figures of merit chosen are **weight, complexity, flexibility/versatility, operating costs, error-proneness, sustainability and viability**. Then, to evaluate the strengths and weaknesses of each design in relation to the chosen figures of merit a Pugh matrix is created and applied to the components propulsion, fuselage, wing and empennage. The propulsion category is further divided into two subcategories architecture (see Figure 2.2) and type (conventional, distributed, tilt). The values and weight factors are determined in an internal workshop with the help of additional literature. Figure 2.2 exemplarily shows the Pugh matrix for the propulsion architecture. The conventional architecture serves as the baseline of the comparison and therefore receives a score of 0 for each figure of merit.

		Weight	Complexity	Flexibility/ Versatility	Operating Costs	Error-proneness	Sustainability	Viability	Total
	Weight Factors	3	2	4	5	5	4	4	**27**
Conventional		0	0	0	0	0	0	0	**0**
Turboelectric		-1	-2	1	1	0	1	-1	**0.1**
Hybrid-electric		-2	-2	3	2	3	2	-1	**1.15**
Full-electric		-3	-1	2	3	3	3	-3	**1.00**

Figure 2.2: Pugh matrix of the propulsion architecture

According to Figure 2.2 a hybrid-electric powertrain architecture should be chosen. A turboelectric approach shows shortcomings in terms of OC and error-proneness which are weightened as the most important figures of merit in accordance to chapter 1. In contrast a full-electric powertrain architecture shows the greatest potential to reduce OC but induces a great weight penalty, which also makes it non-viable compared to the rest.

By taking synergy effects into account, distributed systems offer the best approach in implementing the aforementioned powertrain. Furthermore, a high wing design is beneficial in regards to flexibility and versatility, since it is especially useful for cargo handling and poor ground conditions. Since the U.S restricts the airspeed to a maximum of 250 KIAS below 10 000 ft and a maximum flight time of 99 min is set as a requirement, a pressure cabin would be needed to cover a range of more than 350 NM. Nevertheless, an unpressurized fuselage is favored with the aim of minimizing weight, OC, complexity and error-proneness. With respect to the empennage the V- and U-tail reach the same score in regards to the chosen figures of merit. The V-tail is, however, favored to avoid negative influences by the prop wash of the wing mounted engines.

2.2 Refined Layout

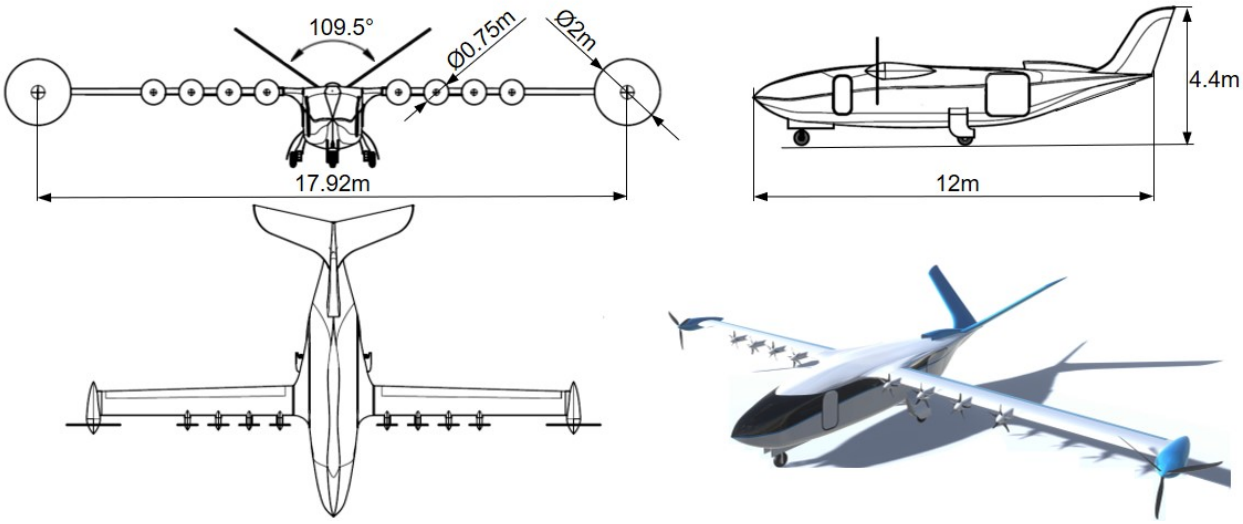

Figure 2.3: *aDEPt*

The *aDEPt* is designed with maximum flexibility and efficiency in mind for thin-haul operations. This includes hub-and-spoke missions as well as point-to-point operations in remote regions that would otherwise not be served by ground transportation. A *Distributed Electric Propulsion* (DEP) approach is chosen and extended by a sensible cabin conversion and loading concept, as well as a morphing wing to further optimize cruise performance.

Additional design freedom in regards to the fuselage can be achieved through the use of composite materials, which also reduce the structural weight. Moreover, this partly compensates the extra weight generated by the hybrid-electric powertrain and batteries.

In combination with an unswept wing the DEP approach allows operations on extremely short runways under poor ground conditions, which not only gives the *aDEPt* bush-plane-like capabilities, but also enables compatibility with future small airparks in otherwise dense suburban areas. Simultaneously, it increases the cruise efficiency as the increased max lift coefficient ($C_{L,max}$) allows a smaller sized

wing while still fulfilling the stall speed requirement. The high wing loading also increases passenger comfort with regard to gusts. Furthermore, in combination with the hybrid-electric powertrain, the reliability is greatly increased. The wingtip propellers offer favorable interaction with the wingtip vortices and therefore decrease drag [3]. The *aDEPt* can fly missions up to 125 NM fully electric and up to 350 NM with a range extender. As battery technology advances, batteries can be gradually replaced by more powerful ones, thus increasing the electrical range, eventually rendering the *Turbo Generator* (TG) obsolete and therefore enforce sustainability. Additionally the *aDEPt* is equipped with the necessary technology for single pilot operations and autonomous cargo flights in all weather conditions. A functional fuselage design, which ensures passenger comfort as well as fast and simple cargo handling, completes the design.

The whole design promotes cost efficiency, which makes thin-haul air travel more viable for airlines and costumers. This helps remote regions to be integrated into the transport network, which not only provides them with the necessary supply goods, but also promotes industry therefore ultimately increasing the inhabitants standard of living.

3 Design Overview

Beginning with the initial sizing, the component sizing has to be done iteratively to meet all performance requirements. Furthermore, some adjustments to the general design methodology have to be made to account for DEP. In order to manage the large amount of data and to be accountable for the numerous dependencies of individual design steps, the design is carried out with the help of numerous self written programs authored by the design team.

3.1 Initial Sizing

A constraint analysis according to Gudmundsson is carried out in order to generate a starting point for the design of the hybrid-electric powertrain and wing [17].

An initial *Maximum Take-Off Weight* (MTOW) of 4 320 kg is assumed. This corresponds to the weight of the Tecnam P2012 surcharged by 20% to account for additional battery weight. Since the *aDEPt* does not have a pressurized cabin, the cruising altitude, cruise speed and climb rate are set to 8 000 ft, 250 KTAS and 1 200 ft/min, respectively. Furthermore, a *Take-Off* (T/O) run of 400 ft is chosen to achieve bush-plane-like flexibility. In order to accomplish this,

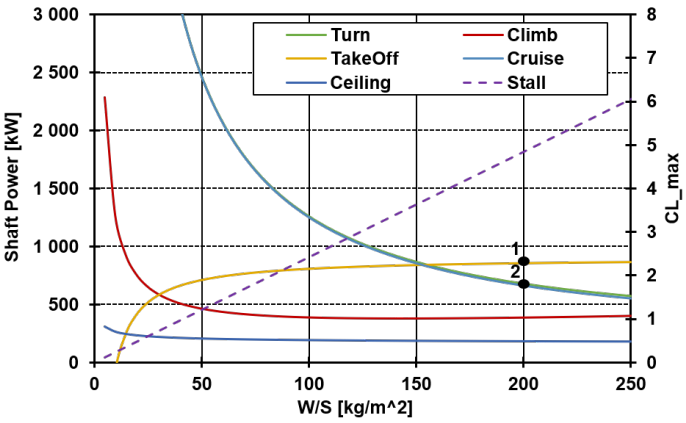

Figure 3.1: Constraint analysis of the *aDEPt*

a stall speed of 50 knots is applied based on the data from NASA's SCEPTOR concept [33]. Figure 3.1 shows the corresponding constraint diagram.

Since DEP serves as an active high lift device, higher wing loading (W/S) compared to conventional aircraft is feasible as a measure to increase cruise efficiency and passenger comfort. A W/S of 200 kg/m^2 is selected taking into account structural and space-related reasons. Consequently a $C_{L,max}$ of 4.85 is required to meet the stall requirement. This serves as a constraint for the *High Lift Propeller* (HLP) design. To meet the power requirement a total shaft power of 860 kW is needed (point 1 in Figure 3.1). However, since the batteries can be used as a buffer for high energy demands, the TG can be scaled down. This leads to a second design point at 662 kW near the requirement for cruise and sustained turn.

3.2 Hybrid-electric Powertrain

The design of the hybrid-electric powertrain is determined by the designated mission profile, especially by the targeted electrical mission. Starting with the values from the initial sizing energy calculation has to be done iteratively in accordance with the optimization of the overall design ultimatly leading to the values seen in Figure 3.2.

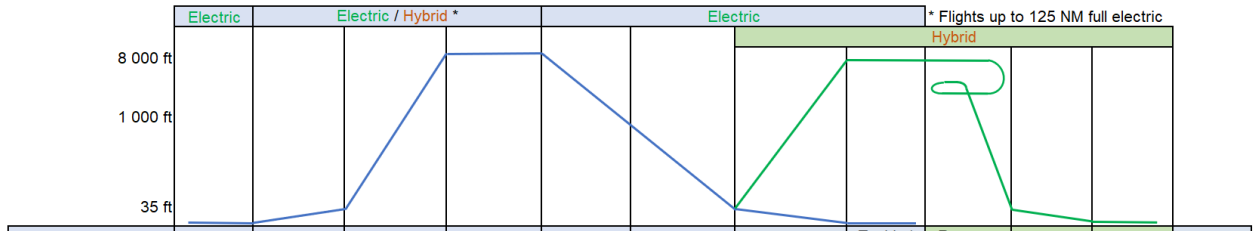

Mission Phase	Taxi out	T/O to 35 ft	Climb to FL80	Cruise	Descent	Final Approach	Landing | Reserve Climb	Taxi in | Reserve Cruise	Reserve Holding and	Reserve Landing	Reserve Taxi in	Avionics
Time [min]	2.00	0.13	6.66	Up to 78	7.74	2.43	0.13 | 6.66	2.00 | 15.6	53	0.13	2.00	-
Rate of Climb [ft/min]	-	-	1 200	-	-	-	- | 1 200	-	-	-	-	-
Rate of Climb [m/s]	-	-	6.1	-	-	-	- | 6.10	-	-	-	-	-
Airspeed [kts]	-	53.46	101.08	250.00	250 - 91.36	91.36 - 58.32	58.32 | 101.68	- | 250	250 - 58.32	58.32	-	-
Airspeed [m/s]	-	27.5	52.00	128.61	128.61 - 47	47 - 30	30.00 | 52.00	- | 128.61	128.61 - 30	30	-	-
Battery energy [kWh]	6.34	2.71	58.97	163.26	9.60	22.01	1.23	6.09				16.22
Fuel consumption [kg]				142.3			23.90	41.09	147.24	0.50	6.10	17.87

Figure 3.2: Mission profile

The *aDEPt* cruises at an altitude of 8 000 ft where only the *Cruise Propellers* (CP) have to be powered. To reduce drag the HLPs are folded back during all mission phases except T/O as well as at the beginning of climb and the end of approach where the *aDEPt* would stall without the lift increase provided by them. Because of the high L/D descent is possible with minimal energy consumption. During the final approach the HLPs are used to lower the stall speed while the *aDEPt* gradually decelerates. In this phase the CPs provide drag through windmilling and/or reverse thrust to enable deceleration even though the HLPs are at full power [32]. In case of a go-around an alternate airport can be reached at a distance of 100 NM. Additionally, a final reserve of 45 min (holding) is provided.

3.2.1 System Architecture

The *aDEPt* focuses on a high lift coefficient at low speeds to allow operation from short runways, while ensuring optimum L/D and maximum drive train efficiency. For this purpose, several electric drives similar to the *SCEPTOR* are used [6]. The engine sizing is carried out according to Stoll et. al. and results in the following motor configuration [48]:

- Two cruise motors with 267.5 kW power and a propeller diameter of 2.0 m
- Eight high lift motors with 55 kW power and a propeller diameter of 0.75 m

For the CPs a double motor configuration as depicted in Figure 3.3 is used to increase redundancy and decrease the loss of thrust in case of a motor failure [45].

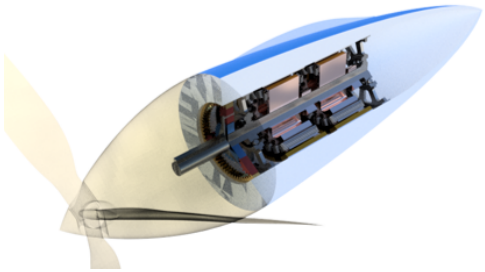

Figure 3.3: Double motor layout

The complete electrical system architecture features a redundant interconnection mode in which two independent controllers and three spatially separated battery packs are used. This guarantees reliability in the event of fire outbreak or electrical issues [24]. Figure 3.4 illustrates said architecture including the efficiencies of the individual components as proposed by literature [21].

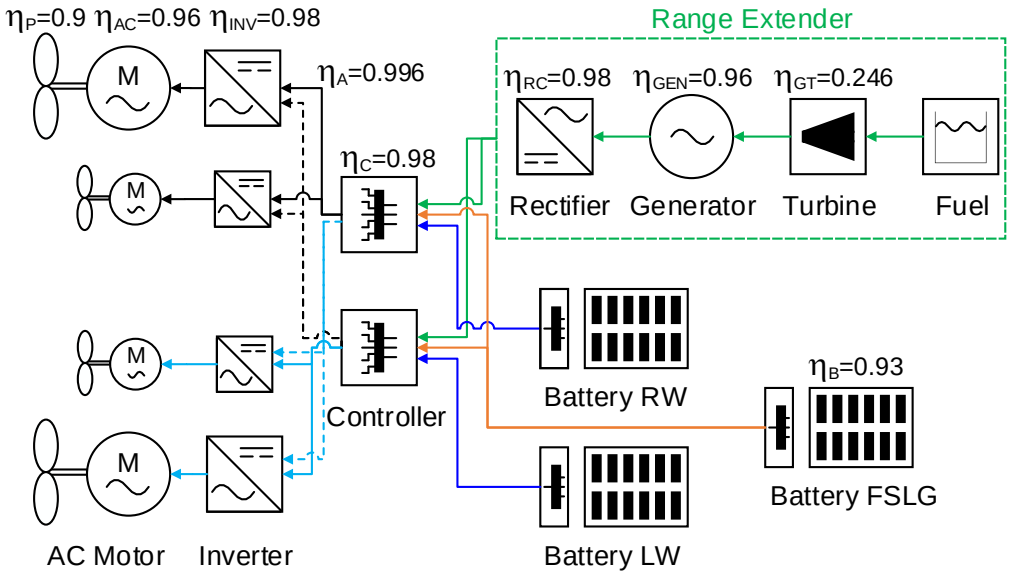

Figure 3.4: Powertrain architecture

For missions within the scope of the design mission, a degree of hybridization of one will be achieved. For longer missions the range extender configuration can be used (see Figure 3.4). A gas turbine and a mechanically coupled generator produce electricity for the engines. The design case as well as the operating point for the turbine enable significant higher efficiencies (see Section 3.2.3).

3.2.2 Battery

Batteries deliver a major part of energy for the flight mission. For the maximum range of 350 NM, they support the TG in all flight phases, especially during T/O.

A demanded design mission of 125 NM should be flown fully electric. This corresponds to about 80% of CA's total flights as well as 98% of their flights not subsidized by the EAS program in 2016 (see Figure 1.1) [59]. The required power output of the batteries is derived from this flight mission, including all flight phases as well as taxiing. Furthermore, they also replace the *Auxiliary Power Unit* (APU).

The most important parameter for the design of the batteries is the available gravimetric energy density. According to Stoll a gravimetric energy density of 400 Wh/kg until the year 2025 is realistic, which is why this value is applied to determine the battery weight [48]. Based on the required power per flight segment and the efficiencies of various components in the powertrain (see Figure 3.4), the required energy per flight segment can be obtained (see Figure 3.2). The resulting battery data is listed in Table 3.1.

Data	**Unit**	**Value**
Gravimetric energy density	$[\frac{Wh}{kg}]$	400
Volumetric energy density	$[\frac{Wh}{l}]$	300
Total energy	$[kWh]$	315.07
Weight	$[kg]$	787.68
Volume	$[m^3]$	1.05

Table 3.1: Major battery data

The total energy requirement results in 315.07 kWh including a safety margin of 10% to consider possible perturbations during flight. Thus, the total battery weight amounts to 787.68 kg. In addition, Kreimeier cites a volumetric specific energy density of 300 Wh/liter, which results in a battery volume of 1050.24 liters (1.05 m^3) [24].

The batteries are located in the fuselage as well as in the inner parts of both wings. To ensure that the required power of the batteries is available for the flight, the batteries in the fuselage are mounted in such a way that they can be replaced easily in order to have fully loaded batteries if needed. The battery units in the wings are scaled in such a way that they can be fully charged with two 150 kW direct current chargers in the available turnaround time. This charging power is currently emerging in the automotive industry and provided by *Ground Power Units* (GPUs) commonly used aviation. In order to dissipate the generated heat during charging, which also arises at increased loads in flight, a liquid cooling system is used [21].

3.2.3 Turbo Generator

Current and projected energy densities of batteries for 2025 make it infeasible to operate fully electric airplanes with short T/O capabilities like the *aDEPt* at typical commuter flight ranges. To combat this issue a TG powered by kerosene is installed in the aft.

The TG provides enough power to function as a range extender for all missions longer than 125 NM including the reserve mission in case of an aborted landing.

Since batteries bridge the power difference between T/O and the remaining flight phases the TG can run close to its design point the whole flight. This drastically reduces kerosene consumption and emissions. The placement of the TG incorporated in the aft and the use of a smaller gas turbine also greatly reduces noise levels. For reference the PT6A-41 is used (see Table 3.2). This gas turbine complies with the calculated power requirement. Additionally the PT6A-41 is one of the most common engines, which makes maintenance and servicing simple and cheap [9].

Data	**Unit**	**Value**
Weight	$[kg]$	182.8
Max. Diameter	$[mm]$	483
Length	$[mm]$	1701
T/O Power	$[kW]$	634
T/O PSFC	$[\frac{kg}{kWh}]$	0.339
Cruise Power	$[kW]$	598.7
Cruise PSFC	$[\frac{kg}{kWh}]$	0.306
Efficiency	$[-]$	0.246

Table 3.2: Specifications of PT6A-41 [9]

Looking beyond 2025, the TG can easily be replaced by a fourth separated battery pack in the aft allowing the *aDEPt* to fly its maximum range fully electric. A replacement of the TG would be feasible once gravimetric energy densities reach 950 Wh/kg.

3.3 Fuselage and Cabin Design

The *aDEPt*'s fuselage and cabin design is characterized by a focus on versatility and adaptability to client requirements. Keeping low turnaround time requirements in mind, the chosen concept makes the cabin conversion between cargo and passenger missions possible without removing or adding any components at the local airport. Aside from decreasing turnaround times, this also has the advantage that components, such as seating, do not have to be stored at the local airport or hub. Subsequently, this enables the *aDEPt* to fly point-to-point mission models varying freely between passenger and cargo missions versus solely hub-and-spoke missions.

3.3.1 Passenger Configuration and Fuselage Sizing

Considering the elongated fuselage form, the seating layout for nine-passenger capacity is limited to only few sensible options. As such, a single-aisle, four left, five right layout is chosen with enough space in the rear of the plane to place baggage. The fuselage sizing takes into account a 864 mm (34 in) seat pitch and a 1 600 mm cabin width. This corresponds with economy seat spacing and offers ample aisle space for quick and comfortable boarding and disembarking [17].

In the absence of a pressurized cabin, the fuselage cross-section is modified to fit the constraints provided by the design passenger and cargo missions. The fuselage length is derived from real-world constraints as prescribed by Raymer, ergo the sum of cockpit, cabin and luggage compartment lengths as well as the length needed for shaping of the tail and nose [39].

The cabin dimensions are compared to the reference aircraft in the *aDEPt*'s design process to assure that realistic values are used. Using these dimension and assuming sufficient space for the cabin floor, skin- and structure thickness and landing gear storage, a basic fuselage form is determined. Figure 3.5 depicts a split view of the fuselage crosssection in passenger and cargo configuration. Further refinement of the fuselage shape takes into account the aerodynamic properties. Junctions between the fuselage and wing are gradual, minimizing induced drag, and designed with a geometry similar to a lifting body to optimize the incident flow at the empennage. In order to obtain an aerodynamic fuselage with sufficient cabin space for the comfortable transport of passengers and cargo, numerous simulations with different cross-sections over the fuselage length are carried out with *OpenFOAM*. The large, cargo compatible fuselage makes it possible to design the landing gear to retract into the fuselage to further reduce drag.

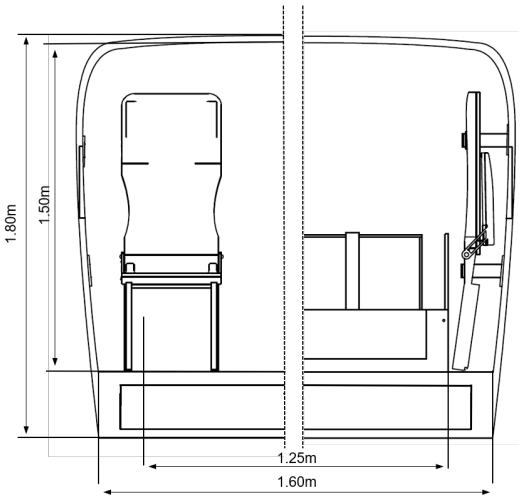

Figure 3.5: Crosssection in passenger- (left) and cargo configuration (right)

(a) Seymourpowell morph [47]

(b) Passenger setting

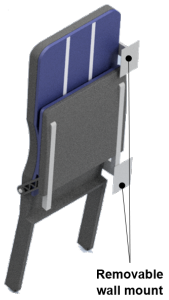

(c) Cargo setting

Figure 3.6: Seating concept

The seat design seen in Figure 3.6b and 3.6c is an adaptation of Seymourpowell's Morph seating concept (see Figure 3.6a). This concept uses fabric made of high-tensile fibers stretched over retractable railings to adjust comfort and partitioning of the three-abreast seat bench. The adapted system offers the same high level of comfort, due to the adjustable design and hammock-like seating feel, while offering an excellent opportunity for minimizing seat-dimensions in a stowaway configuration (see Figure 3.6c). For the general seat design, anthropomorphic data for a 95th percentile male is used along with the baseline for airline seat dimension comparison to assure realistic values for the *aDEPt* [1, 17, 35].

Additionally, due to the collapsible seat volume, material weight is reduced in the seat design. The *aDEPt*'s seating system features a mounting port for a carrying hinge that eases the stowaway and set-up of the seats. The possibility of decoupling the hinge and seat gives the carrier the option of removing the seats between passenger and cargo missions to avoid dead weight during the flight. In this case, the lightweight and foldable design remain beneficial for the cabin conversion.

3.3.2 Cargo Configuration

In the cargo configuration, the fuselage is designed to hold up to four standard GMA or EPAL2 pallets, or five EPAL1 pallets on which the cargo load can be evenly distributed, as all three standards are widely used on the international market [20]. Designing around these standardized dimensions decreases turnaround times and OC during cargo missions compared to having a proprietary pallet system. This is because depalletizing and repalletizing cargo becomes unnecessary, though the use of plastic pallets is advised in order to save weight [38]. Furthermore, the cargo volume capacity of the *aDEPt* is estimated at 7.33 m^3, 6.36 m^3 of which can be directly loaded onto the pallets as constrained by the loading door. The crates can be secured atop the pallets once in the cabin to make use of the remaining space. Soley the loaded pallets achieve a chargeable weight of 157 kg/m^3, improving on the volume capacity of the chargeable weight average of 167 kg/m^3 prescribed by the *International Air Transport Association* [43]. Using mail crates in the remaining space, for instance, further boosts the chargeable weight average of the volumetric cargo capacity to 136 kg/m^3.

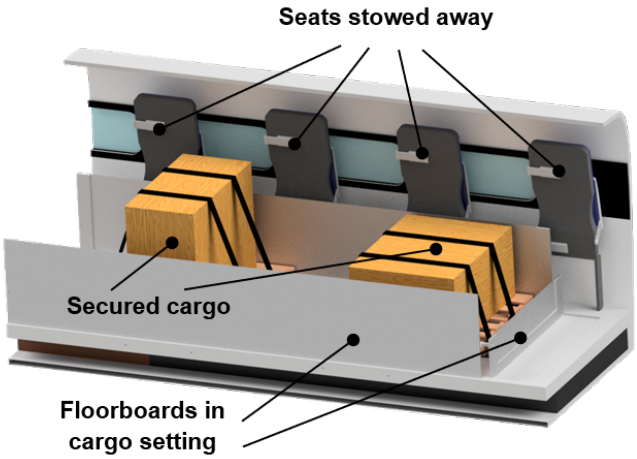

Figure 3.7: Cabin in cargo configuration

Altogether, this implies that air freight with the *aDEPt* could be more lucrative, be offered at cheaper rates, or simply contain more low density freight without superceding the maximum cargo load.

This might be of special interest for online mail order companies, whose packages, based on DHL product specifications, fall far below 167 kg/m^3 [10]. The cargo cabin configuration is assembled by setting the seats in a stowaway position, turning the floorboards up in a 90° position and lastly setting the floor supports down that would otherwise provide an even load distribution on the sandwich-structure floor boards. This reveals the roller system below, on which the cargo pallets are loaded, positioned, and secured via restraints between the rollers.

3.4 Morphing Wing

The *aDEPt's Trailing Edge* (TE) movement is realized by electro-mechanical actuators in combination with wire rope hoists, as tested by NASA on a Gulfstream III in 2015 [61]. The TE can be moved in accordance to the material limits between 9° (up) and 40° (down) with an adjustment rate of 30 °/s [14]. Sensors in the material provide information about the position of the flap and the condition of the material. As shown in Figure 3.3 a gap between flap and wing influences the lift coefficient and L/D-value. In order to fly more efficiently a higher L/D-ratio is desirable. The smooth transition

between wing and flap allows a more friction-free flow compared to conventional flap systems, thus increasing the L/D (see Figure 3.9). By using a morphed TE fuel savings between 3% and 5% can be achieved in theory [14].

Gap	C_L	C_D	L/D	C_{Lmax}
1% cord length	0.26	0.023	11.13	1.97
0% cord length	0.26	0.018	14.06	1.91

Table 3.3: Influence of a flap gap at 20° flap angle on aerodynamic parameters

The TE incorporates eight multifunctional flaps (four on each side). By exploiting the high adjustment rate, this system combines high-lift devices and ailerons. Due to the large effected area and an independent control of the individual control surfaces the high lift capabilities of this design are suitable for short T/O. Additionally, a steeper and slower approach can be guaranteed, which shortens the landing distance. The low response times of the electrically operated morphing system allows to respond to spontaneous aerodynamic loads like wind shear and gusts and can be controlled to reduce overall material strain. Additionally, it allows the steering of wind conditions to improve passenger comfort [50].

Under certain cruise conditions ice can form. To encounter this, the waste heat from the batteries is conducted through the *Leading Edge* (LE) of the wing. Furthermore microwave de-icing systems are integrated into the LE if the *aDEPt* is flown outside of its electrical design envelope.

3.4.1 Performance Analysis

The GAW-1 and GAW-2 airfoils are developed to meet all requirements made on a wing in general aviation. These airfoils combine high lift with low drag, which is important for short T/O distances and efficient cruise conditions. Therefore both airfoils are analysed with focus on cruise, landing and T/O performance as well as space for system integration. In order to calculate the performance of the morphing wing under various conditions the airfoils are morphed with the help of a self-written *Python* script by rotating the mean camber line at 70% relative cord length in steps of 0.5° (see Figure 3.8). The resulting end position and local gradient of the profile line at 70% cord length are used to determine the morphed geometry.

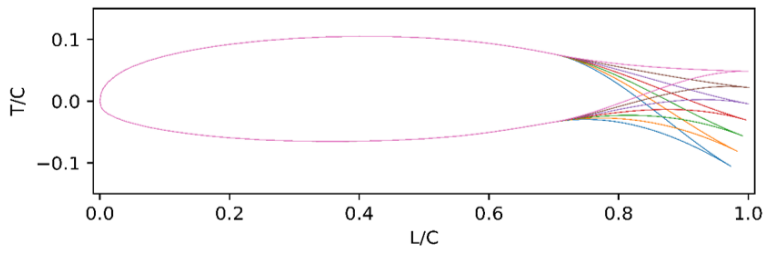

Figure 3.8: Example airfoil GAW-1 morphed in 5° steps between 10° up and 20° down

The aerodynamic characteristics are calculated using *XFOIL* [12]. In Figure 3.9 the wing performance can be seen for a range of C_L values for three different cases. The blue curve (Morphed Profiles) connects the best L/D values achieved at certain C_L-values with the GAW-1 and GAW-2 airfoils with thickness scaling applied to values between 15% and 19%. If one of the two GAW-1 curves lies on the blue curve, this means that the L/D values of this airfoil form the blue curve. This is equivalent to the statement that the airfoil has the best L/D value for this C_L-value.

The chosen speed, altitude and wing loading yield a required C_L-value in cruise of 0.2638. As seen in Figure 3.9 the GAW-1 with a standard thickness of 17% is the best airfoil under cruise conditions. It offers a high $C_{L,max}$ ($C_{L,max} = 2.47$) value with flaps in a 40° position, decent stall speed and high performance during T/O and landing. Furthermore, it provides enough space within the wings for structural parts, batteries and cooling- and de-icing-systems.

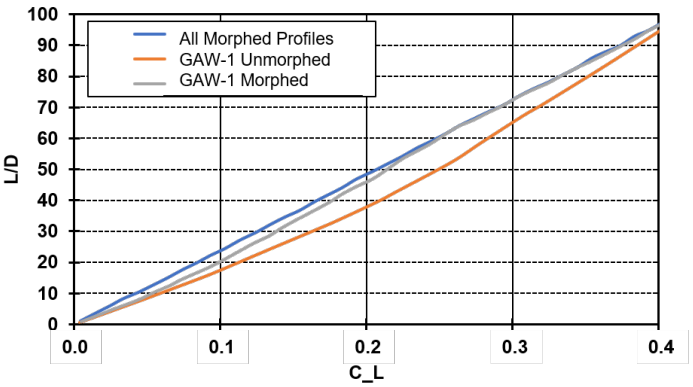

Figure 3.9: L/D over C_L (Re = 8.32e6 M = 0.39)

Regardless of the current aircraft weight or speed the angle of attack can be kept constant during cruise. Therefore, the fuselage creates the minimum drag possible and the L/D-ratio is optimal during the entire flight. For the design passenger mission this results in an L/D of 64.5, compared to a non-morphed wing L/D of 53.7.

3.4.2 Synergy with DEP

The HLPs are installed upstream to the leading edge of the wing increasing the incident flow velocity and hence dynamic pressure at the wing due to the propeller induced velocity. This results in a significant lift increase during low velocity flight, especially during T/O and landing. The CFD simulations conducted with *OpenFOAM* indicate a C_L increase of 2.6 for a stall-speed of 25 m/s. This is in line with Stoll's momentum theory-based approximation [48]. Therefore the blown airfoil achieves a $C_{L,max}$ of 5.6 with a 20° flap angle.

3.5 Empennage

To obtain a V-Tail configuration the horizontal (H) and vertical (S) stabilizer are geometrically designed separately. The corresponding design case for the horizontal stabilizer is the static longitudinal stability at T/O (see Equation 3.1) [37, 28].

$$\frac{S_H}{S} \geq \frac{C_{m0FR,max} + \frac{x_{CGV} - x_N}{MAC} C_{AFR,max} - V_T C_{T,max}}{C_{LH,min} \eta_H \frac{r_H}{MAC}} \tag{3.1}$$

The design case for the vertical stabilizer is directional stability in the event of one-sided damage to the cruise propeller during T/O and a crosswind of $0.2V_S$ (FAR Part 23). If the sensors detect an error of a CP, the computer automatically adjusts the propeller pitch angle of the CP on the opposite side to idle speed, brakes it to a standstill and finally switches it off. This prevents a dangerous influence from the long lever arm. The HLPs have enough thrust to continue the T/O process. In cruise flight, the failure of a CP can be partly compensated by the use of the HLPs on the same side and can therefore be assessed as uncritical compared to T/O.

For a laterally stable aircraft the yaw rate caused by sliding angle β must be positive ($C_{n\beta} \geq 0$) (see Equation 3.2) [50].

$$C_{n\beta} = C_{n\beta,fslg}\beta + C_{n\beta,wing}\beta + \eta_S \frac{\delta\beta_S}{\delta\beta}\beta_{eff}\frac{S_S}{S}C_{Y\beta,S}\left(\bar{X_S} - \bar{X_{CG}}\right) - \frac{\Delta T}{qS}\bar{y_t} \tag{3.2}$$

Subsequently the resulting tail surfaces, which are needed to ensure stability, are combined to a V-tail (V) using the following Equations 3.3, 3.4.

$$S_V = \frac{S_H + S_S}{K_{\Lambda VH}\cos^2(\nu) + K_{\Lambda VS}K\sin^2(\nu)} \tag{3.3}$$

$$\nu = \tan^{-1}\left(\sqrt{\frac{S_S K_{\Lambda VH}}{S_H K_{\Lambda VS} K}}\right) \tag{3.4}$$

$K_{\Lambda VH}$, $K_{\Lambda VS}$ and K are referred to as efficacy factors, while ν indicates the angle of a tailplane page to the horizontal [37].

Table 3.4 summarizes the geometric data of the V-Tail. Both the choice of aspect ratio and the choice of a swept tail guarantee a minimum tail area with maximum stability.

Geometry	Unit	Value
Area	$[m^2]$	8.582
Aspect Ratio	[-]	6.0
Taper Ratio	[-]	0.6
Halfspan	[m]	3.588
Opening Angle	[°]	109.458
Leading edge sweep	[°]	20
Relative rudder depth	[-]	0.3

Table 3.4: Geometry of the V-tail

3.6 Weight and Balance

To estimate the aircraft mass, empirical formulas according to Raymer and NASA's *Flight Optimization System* (FLOPS), as well as specific power ratios for the hybrid-electric powertrain proposed by literature are used [21, 39, 57]. Since no public component mass distributions exist for the reference aircraft, the developed model is verified based on the *Manufacturer's Empty Weight*

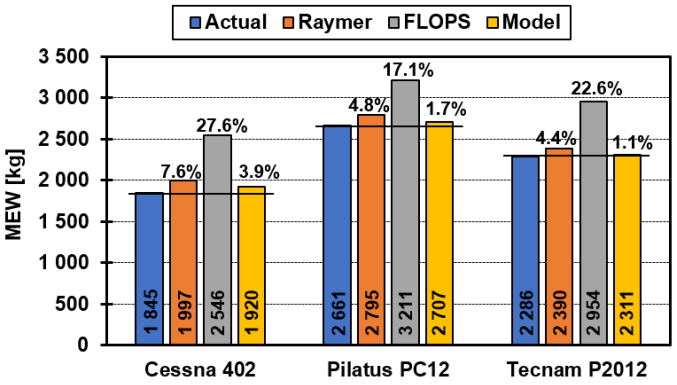

Figure 3.10: Comparison of weight deviations

(MEW) given in the literature to ensure that the implemented model does not deviate further from the MEW than the individual models of the authors.

The model shows great accurancy with respect to the MEW, as shown in Figure 3.10. The percentage values above the columns indicate the deviation from the actual weight. The high mean deviations of the FLOPS model are due to the highly overestimated system weight. This is verified by additionally comparing the weights with the calculated system weights of other models published in literature. Therefore the equations given by Raymer are used to calculate the weight of the individual system components [39]. To account for the additional systems needed to ensure autonomous cargo transport avionic system mass is increased by 50% as a first estimate.

The structural component weight is determined using empirical formulas based on FLOPS as it allows some additional refinements over the equations given by Raymer. To take the cargo loading system into account, the fuselage weight is calculated with the specific formula for transport fuselages. Moreover, the wing weight is calculated using the refined wing model for composite structures [57]. In order to consider the influence of composite on all other structural components, the corresponding factors proposed by Raymer are used [39].

The weight of the individual components of the hybrid-electric powertrain are calculated based on specific power ratios [21]. In contrast, the weight of the propeller is calculated using an empirical formula according to Torenbeek, since neither FLOPS nor Raymer provide a corresponding formula [52]. A detailed mass breakdown of the *aDEPt* can be found in Table 3.5.

Description	**Mass [kg]**
Structure	**973**
Wing	291
V-Tail	61
Fuselage	432
Landing Gear	159
Nacelle	30
Propulsion	**748**
Turboshaft(installed)	239
Electrical components	393
Propeller	75
Fuel System	41
Systems	**403**
MEW	**2 124**
Battery	788
Fuel	379
Max. Payload	1 058
MTOW	**4 349**

Table 3.5: Mass breakdown of the *aDEPt*

In order to ensure sufficient stability and controllability, a static margin of 10% is taken into account during the calculation of the *Center of Gravity* (CG). Additionally, landing gear sizing is conducted in accordance to Gudmundsson [17]. The whole problem is solved iteratively as CG-, mass-, landing gear and stability analysis influence each other.

3.7 Summary and Technology Readiness Level

Table 3.6 summarizes the *aDEPt's* key parameters resulting from the design process. The given values for T/O, landing and noise are further discussed in chapter 4. Additionally, the used key technologies with their current *Technology Readiness Levels* (TRL) are presented in Table 3.7. Since the year of

commissioning is set to 2025, technologies with a TRL of less than 6 were not considered in the design process described in chapter 2.

The particular DEP configuration chosen has been part of NASA research since 2014 [49]. As of 2019 the NASA X-57 Maxwell project is in its third out of four modification stages, which is expected to be finished by mid-2020 [30]. Morphing wing technology has been successfully tested with a Gulfstream III by the NASA [29]. Additionally *FlexSys* has been researching compliant systems for almost 20 years [14].

The assumed battery density of 400 Wh/kg can be reached with solid state batteries. The *Fraunhofer Institute for Silicate Research* (ISC) is already testing several prototypes and predict production readiness for the year 2020 [23]. Furthermore, Toyota intends to install solid state batteries in electric cars as early as 2025 [16].

Increasing single pilot performance has already been a major point of research in scope of the *Small Aircraft Transportation System* (SATS) conducted by the NASA in 2008 [54]. Unmanned autonomous flights are under heavy research by military institutions all over the world. Apart from military uses Boeing researchs autonomous systems in relation to air taxis [13]. It should be noted that, while autonomous cargo transports may be possible by 2025 with the technologies at hand, this does not apply to autonomous passenger transport, since it can be assumed that to overcome the distrust of the passengers and certification authorities the technology has to be proven for years without any major incidents.

Parameter	**Unit**	**Value**
MTOW	[kg]	4 349
Battery mass	[kg]	787.68
Fuel tank	[l]	550
PAX	[-]	9
T/O-Distance	[m]	158.99
Landing distance	[m]	158.84
Cruise speed (max.)	[kts]	250
Stall speed	[kts]	49
Noise*	[dB]	64.35
Max range	[NM]	350
Electrical range	[NM]	125
Alternate airport	[NM]	100
Holding	[min]	45
Length	[m]	12.0
Span	[m]	19.92
AR	[-]	15

* at flyover point

Table 3.6: Summary of key Parameters

Key Technology	**TRL**	**Reference**
Morphed Trailing Edge	8	[14], [22], [29]
DEPs	6	[49], [6]
Single-Pilot Cockpit	8	[54]
Autonomous Flight (unmanned)	6	[13, 40]
Battery	6	[16], [23]
Microwave De-icing	6	[58]

Table 3.7: Overview of the TLRs of used technologies

4 Performance Analysis

This chapter discusses the aircraft performance with focus on T/O, landing, noise and cruise performance. To determine the overall performance of the aircraft, the wing including nacelles and the influence of the HLPs as well as the fuselage are simulated in *OpenFOAM*. The CFD model of the wing is validated against Stoll's momentum theory-based approximation as described in section 3.4.2. Subsequently, the individual aerodynamic components of the aircraft are assembled in accordance to Gudmundsson [17].

4.1 Take-Off and Landing

T/O is calculated by solving the equation of motion as proposed by Gudmundsson [17]. For T/O a flap setting of 20° as well as maximum thrust of the HLPs and CPs is considered leading to a mean acceleration of more than 5 m/s^2. This enables a very short ground run of 65 m and allows the *aDEPt* to overfly a height of 35 ft within 158.99 m. For landing, flaps are at their full setting (40°), while the HLPs are at full thrust to enable the low stalling speed of 25 m/s. To keep the velocity constant the CPs already provide reverse thrust in the last segment of the final approach. As soon as the airplane lands on the ground, the flaps move up to 9° to create downforce, while the CPs deliver maximum reverse thrust. This configuration yields a total landing distance of 158.84 m.

4.2 Noise

The *aDEPt* features low noise emission. This is supported by the DEP approach, which emits significantly less engine noise, and by stowing the TG in the aft. In order to estimate aircraft noise, the individual noise contributions from the most crucial components propeller, fuselage and wing are calculated individually. To predict the far-field propeller noise, a semi-empirical approach according to Marte et. al. was used [26]. Based on the motor power, a reference *Sound Pressure Level* (SPL) is determined for each drive. This SPL is then corrected by the number of blades, rotational speed, directional characteristics and attenuation due to spherical spreading of sound. Selfridge et. al. has proposed an equation that can be used to calculate the harmonic distribution of sound up to the 10th order [44]. Depending on the loading sound frequency this leads to ten different SPL's which have to be corrected for atmospheric absorption.

SPL [dB]	**Segment 1**	**Segment 2**
Propeller	50.74	62.70
Airframe	42.20	59.34
Aircraft	51.31	64.35

Table 4.1: SPL at segment one and two

The airframe noise is determined using the approximation proposed by Gibson [15]. As specified in procedure 24 CFR Part 36 Appendix G two SPLs are calculated at the relevant flyover points in segment one and two (see Table 4.1). This results in a peak SPL of 64.35 dB.

4.3 Cruise Performance

The *aDEPt* uses multiple systems to enhance cruise performance and therefore reduce the impact of the additional battery weight on energy consumption. This allows efficient cruise operations at 250 KTAS and below, which is shown in Figure 4.1 in terms of L/D and electrical range as a function of cruise speed. The given electrical range incorporates a 10% battery power reserve for safety reasons.

The majority of today's commuter flights are performed by aircraft, which are restricted to a cruise speed of about 200 kts [59]. At this speed the *aDEPt* excels with a *L/D* of 23.9 and an electrical range of 163 NM, which for example covers about 90% of CA's currently flown missions (see Figure 1.1). In addition, with the TG, a total range of 280 NM can be achieved within the specified time span of 99 min, with a consumption of only 43.5 kg of fuel. The outlined mission, the cargo- and passenger design missions as well as the maximum range mission are summarized in Table 4.2, respectively. The design missions aims to achieve the highest possible utilization while taking the requirements given by the NASA/DLR into account. Since the cargo mission requires a shorter turnaround time, it can be flown more efficiently at a slower cruise speed.

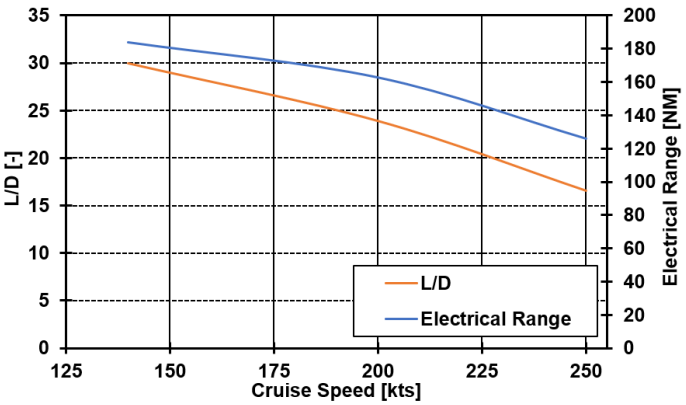

Figure 4.1: Cruise speed performance

Parameter	Unit	Mission Profile			
		Max. Range	Passenger	Design Passenger	Design Cargo
Cruise speed	[kts]	250	200	250	140
L/D	[-]	16.6	23.9	16.6	29.9
Range	[NM]	350	280	120	120
Max. Range (electr.)	[NM]	125	163	125	184
Flight time	[min]	99	99	45	60
Fuel consumption	[kg]	142.3	43.5	0	0
Turnaround	[min]	45*/30**	45	45	30

*passenger **cargo

Table 4.2: Overview of the aDEPts performance within different missions

5 Avionics and Autonomy

Compared to traditional FAR Part 23 aircraft, single-pilot and autonomous operations require additional avionic systems. These systems must increase the pilots situational awareness without inducing information overload and enable safe autonomous flight. Additional requirements for the *aDEPt*'s use case include the flight in *Instrument Meteorological Conditions* (IMC) under *Instrument Flight Rules*

(IFR) as well as flight into known icing conditions. For training purposes the *aDEPt* can still be flown by two pilots.

5.1 Single Pilot Operation

For single pilot operations the workload of the pilot has to be maintained at acceptable levels. Many approaches for single-pilot operations have been pioneered by the military and can now be implemented in civilian operations. To reduce the workload of the pilot, the *aDEPt* is designed as a fly-by-wire plane. This allows the installation of flight augmenting software and prevents the plane to be flown outside its design envelope. By fusing the input of several sensors into a comprehensible overall picture the pilot can judge the planes status and flight environment. Each critical system is triple redundant.

In order to present the sensor data clearly, the cockpit is designed as a glass cockpit with a *Head-Up Display* (HUD). The HUD can display information about the flight attitude, airspeed, height and route [18, 56]. With IR-cameras, a picture of the environment during low or no visibility flight can be generated and projected onto the HUD [7]. The plane position is determined via a satellite navigation system augmented with *European Geostationary Navigation Overlay Service* (EGNOS) and *Wide Area Augmentation System* (WAAS) allowing landing in IMC without an *Instrument Landing System* (ILS) at the airport [54]. Additionally, the radar scans for landmarks to augment the accuracy of the navigational data. To prevent mid-air collisions, the *aDEPt* is equipped with *Automatic Dependent Surveillance - Broadcast* (ADS-B) and is therefore capable of evading other planes without control input by the pilot.

By integrating an *Automatic Ground Collision Avoidance System* (AUTO-GCAS), the *aDEPt* prevents controlled flight into terrain in case of an incapacitated pilot and prepares the plane to be remotely landed. The AUTO-GCAS collects data primarily via *Terrain Following Radar* (TFR) whose function is to provide data for climb and approach [4]. The radar is also used to prevent bird-strike at T/O by scanning the airspace for birds or drones. Data generated by inertia sensors are used to keep the plane within its designed flight envelope as well as smoothing the ride by actively actuating the morphing TE in case of disturbances.

5.2 Autonomous Flight

To ensure autonomous flights a strong data connection is needed. For this the *aDEPt* is equipped with a UHF radio communication system as well as a high bandwidth satellite communication system for areas where no UHF coverage is available. The routes are predetermined by waypoints set before T/O during the mission planning [25]. Inertia sensors are used to detect irregularities during the flight. To prevent GPS spoofing a triple redundant inertia guidance system is installed. Additionally the radar can backup the GPS data by comparing the planes surroundings with known topographical data. The inertia guidance system is calibrated every time at its parking position on an airport.

To prevent the *aDEPt* from being abused by unauthorised actors the data transfer between the aircraft and the remote operator has to be encrypted with a strong encryption such as AES 256. A key is generated before every flight using e.g. an authenticated Diffie-Hellman key exchange. The logic and compute resources of this key exchange are in a hardware key module which can be exchanged, when stronger encryptions become necessary. Due to the short validity of an exchanged session key the risk of an aircraft being controlled by unauthorised actors is mitigated, as long as they can not perform significant hardware modifications on the aircraft or the controller itself. Nevertheless, for safety reasons a *Ground Pilot* (GP) is required, who can gain emergency access to the *aDEPt* [24, 48]. However, since the GP only provides stand by service he can be responsible for several existing aircraft at once.

Besides the technical challenges, passenger acceptance is the greatest obstacle for autonomous flying. Studies show that people offer great distrust against autonomous and even remotely controlled systems [40]. Therefore, autonomous flight missions are initially limited to cargo missions at night until a certain level of customer confidence is reached. Since operations with FAR Part 23 certified aircraft have a significantly higher accident risk than those with FAR Part 25 certified aircraft, it can be assumed as a first indication that autonomous passenger flights will not be possible until a similar accident rate as with FAR Part 25 certified aircraft can be achieved [60]. Nevertheless, autonomous cargo missions at night in the same aircraft that carries passengers throughout the day could help overcome distrust and discomfort earlier.

Since a fully autonomous mission does not require a cockpit crew, both the pilot seat and instrument panel can be removed. This saves weight and creates additional space. However, as the carriage of more than 9 passengers would require certification to FAR Part 25 instead of Part 23, this space cannot be used for the carriage of additional passengers, by todays standards. Instead the accomodation scheme could be changed. At the passengers request, the separate cockpit area could be equipped with more comfortable seating and entertainment at a small extra charge. Having no pilot on board also opens up additional possibilities with regard to the operating concept, especially in relation to on demand air travel, as the operator is not tied to the pilots location.

6 Operation Concept

Because of its *Short T/O and Landing* (STOL) abilities and avionic equipment the *aDEPt* can service almost every airport worldwide only restricted by its span of 19.92 m. Airlines can therefore use more than 18 000 airports in the USA alone to build an air transport network that provides air services to remote areas [54]. To use the *aDEPt's* electrical capabilities, facilities for the recharge and/or swap of battery packs are needed. The ongoing research and support in electrical ground transportation, however, will help to integrate a large part of these airports into the electrical transportation network. This applies in particular to future small airparks, who might emerge in otherwise dense suburban areas. This promotes the opportunity of numerous *Operating Concepts* (OpCo) to ensure a high utilization.

6.1 Exemplary 24-hour Operational Concept

The increasing demand in the thin-haul segment has not only been determined by CA on its own missions, but is also investigated by various authors. The research conducted indicates that demand for thin-haul flights will increase significantly in the future, if OC fall to a certain level [42, 46, 60]. This opens up the possibility for OpCos like the one depicted in Figure 6.1, which is based on the given design mission (see Table 7.1). This OpCo focuses on the maximum number of flights during a 18 hour utilization period. Taking the given turnaround and mission requirements into account, the *aDEPt* can fly up to 8 passenger and 4 cargo missions within the given 18 hour time frame.

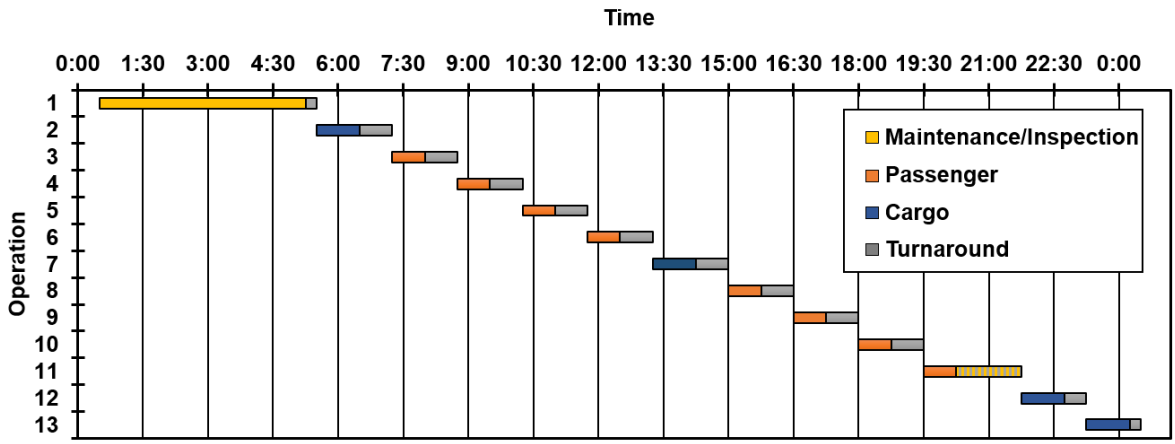

Figure 6.1: Gantt chart of an exemplary operational concept

Because of its sensible cargo loading concept the *aDEPt* can start with a piloted cargo mission early in the morning (5:30) outside of passenger rush hours. At the airport the cargo is unloaded and the floorboards and seats are folded back into passenger configuration easily during the scheduled turnaround. Subsequently, passengers who seek connection to the next major city can be conveniently transported. In order to avoid any downtime outside of passenger rush hours, an additional cargo mission can be flown in between passenger missions. Since the last flight of the day must be performed to the home airport of the *aDEPt* for crew reasons, the seats can be removed and stored away after the passengers disembark. Additionally, the airplane undergoes light inspections to prepare it for autonomous cargo missions. This shall be done within 90 min (including turnaround), which is enough time to fully charge the batteries with todays charger capacity. Since no passengers or pilots are required for autonomous cargo missions they can be flown at a steeper climb rate as well as at an higher altitude to reduce noise and avoid icing conditions. At night the *aDEPt* can undergo light maintenance/inspections which includes the check of functionality of the TG and batteries as well as virtual tests of the autonomous system.

Other possible OpCos include flying all cargo missions at night (autonomous), or, in absence of passenger demand, additional cargo missions in the afternoon.

6.2 Ground Handling

After landing the *aDEPt* is connected to the GPUs as fast as possible. Charging the wing batteries makes up a substantial part of the turnaround time as they are designed to be charged within 25 min. For longer flights that rely on the use of the range extender refuelling can be done simultaneously. Since its not possible to fully charge the batteries with todays charger output of around 150 kW the battery cells within the fuselage can be swapped if needed. Due to safety concerns this cannot be done while the plane is refuelling. Afterwards the cabin is cleaned and passengers board the aircraft through the rear loading door. In case of cargo transport standard pallets can be easily loaded through the rear door with the help of a forklift. The wide aisle in the cabin as well as ground clearance due to the high-wing design ensure fast boarding and evacuation times in case of an emergency.

7 Cost Estimation

Life Cycle Costs (LCC) are commonly divided into *Design and Development Costs* (DDC), *Production Costs* (PC), *Operating Costs* (OC) and *Disposal Costs* (DC). However, DC are typically not considered, as they represent an insignificant share of the total life cycle costs and are typically not considered when a purchase desicion has to be made. The Tecnam P2012, Cessna 402 and Pilatus PC12 are used as reference aircraft [8, 34, 51]. All aircraft are compared on basis of the design mission presented in Table 7.1. To account for inflation, all costs are adjusted to 2018-USD using the corresponding *Consumer Price Index* (CPI).

Parameter	Unit	Value
Range (complete)	[NM]	120
Range (electrical)	[NM]	120
Flight time	[min]	45*/60**
Fuel consumption	[kg]	0
Turnaround	[min]	45*/30**
Passenger missions/day	[-]	8
Cargo missions/day	[-]	4
workload days/year	[-]	300

*passenger ** cargo

Table 7.1: Design mission

7.1 Life Cycle Costs

Acquisition Costs

The Eastlake business model, as proposed by Gudmundsson, is used to calculate the acquisition costs of the aircraft, since the general aviation model proposed by the same author calculates unrealistical low values for the reference aircraft whose purchase prices are known [17]. The wrap values recommended by Gudmundsson are inflation-adjusted to \$100, \$66 and \$58 per hour for engineering, tooling, and manufacturing, respectively. Gudmundsson further suggest avionic costs of \$60 000 which are increased to \$240 000 to account for the additional equipment needed to ensure autonomous flights. To calculate the electrical powertrain components the cost values proposed by Stoll are used [48]. Nykvist and Nilsson propose Battery costs of \$100/kWh to \$150/kWh for the year 2025 [31]. The upper bound of \$150/kWh is set as a conservative projection. Additionally, the quantity discount factor, which

represents the learning curve in the production cycle, is set to 0.9 which poses the middle ground between a very optimistic and a very conservative scenario.

The resulting *List Price* (LP) amounts to **$3 258 056** for a profit margin of 15%. This places the *aDEPt* between the P2012 ($2.7M) and the PC12 ($4.963M). This is reasonable, since the cost model shows the greatest sensivity in terms of structural weight and maximum airspeed, both of which are parameters where the *aDEPt* is closer to the P2012 than the PC12. The increased costs in relation to the P2012 are primarily because of composite structures and the additional avionics and powertrain costs.

Cash Flow Analysis

To reflect the profitability of the aircraft program for the manufacturer, the *Net Present Value* (NPV) and *Break Even Point* (BEP) are determined. The NPV can be calculated with Equation 7.1.

$$NPV = -\frac{DDC}{PR} + \sum_{t=1}^{T} \frac{LP - PC}{(1+i)^t} \tag{7.1}$$

The *Production Rate* (PR) is set to 800 aircraft over $T = 8$ years, as prescribed by the NASA/DLR. To account for cash flow discounting an interest rate i of 5% is chosen. The NPV results in **$422 251 831**. The BEP is reached at **401** aircraft sold as shown in Figure 7.1.

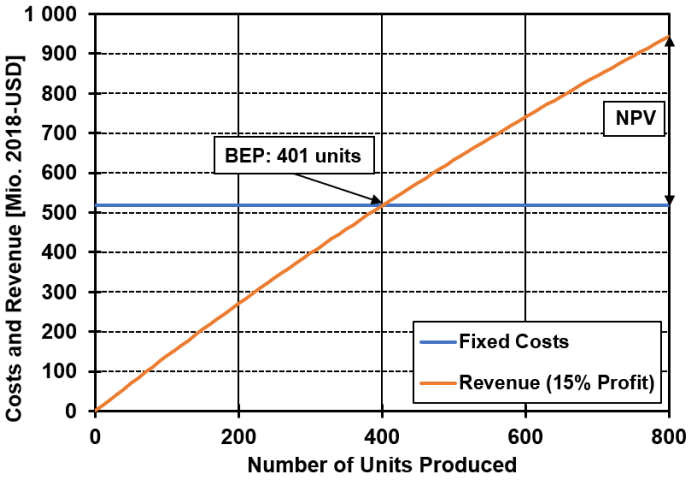

Figure 7.1: NPV and BEP for a 15% profit margin

Operating Costs

The OC are divided into *Variable Operating Costs* (VOC) and *Fixed Operating Costs* (FOC), whereby the VOC include all costs that are only incurred when a flight is operated. To calculate the VOC and FOC the following points have to be considered:

- **Energy Costs** $0.0692/kWh (average 2018 industrial rate) and a charger efficiency of 95%. $4.5/gallon for 100LL fuel (for the reference aircraft) [24, 41].
- **Overhaul:** According to Harish, electric motors will not be overhauled during the operating life of an aircraft [19].
- **Maintenance:** Electric motors and composite airframes require less maintenance. Therefore discount factors are introduced and multiplied with the hourly maintenance cost rate of $140 proposed by Stoll [48]. A cost reduction of 20% for electric motors and 35% for a composite airframe are proposed by literature [5, 36]. This results in a weighted cost rate of $101.5/hour.

- **Labor:** \$40/hour [17]. Since the turnaround times are low, the rate is applied to the complete utilization period instead of just the block time.
- **Fees:** Calculated according to Gudmundsson [17].
- **Battery:** The batteries need to be replaced after 2 000 charging cycles for \$150/kWh [11, 31].
- **Storage:** \$18 000 (upperbound recommended by Gudmundsson) [17].
- **Depreciation:** In addition to the aircraft, a charging station worth \$300 000 is being depreciated over a period of 20 years [2].
- **Insurance:** Calculated according to Gudmundsson [17].
- **Interest:** 6% interest rate. It is conservatively assumed that the entire purchase price needs to be financed over a 10 year loan period.
- **Others:** Ticketing, administration, promotion costs, etc. are considered with a surcharge factor on costs-of-goods-sold (all OC except for capital expenditures) of 10% [24].

The cost model calculates the OC of the *aDEPt* to **\$2.777/NM** (\$336/flight, \$0.309/ASM (*Available Seat Mile*), \$454/flighthour) when operated by one pilot, making it 31.2%, 33.3% and 53.3% cheaper to operate than the P2012, C402 and PC12, respectively. Figure 7.2 shows the individual cost components of the *aDEPt* and the reference aircraft.

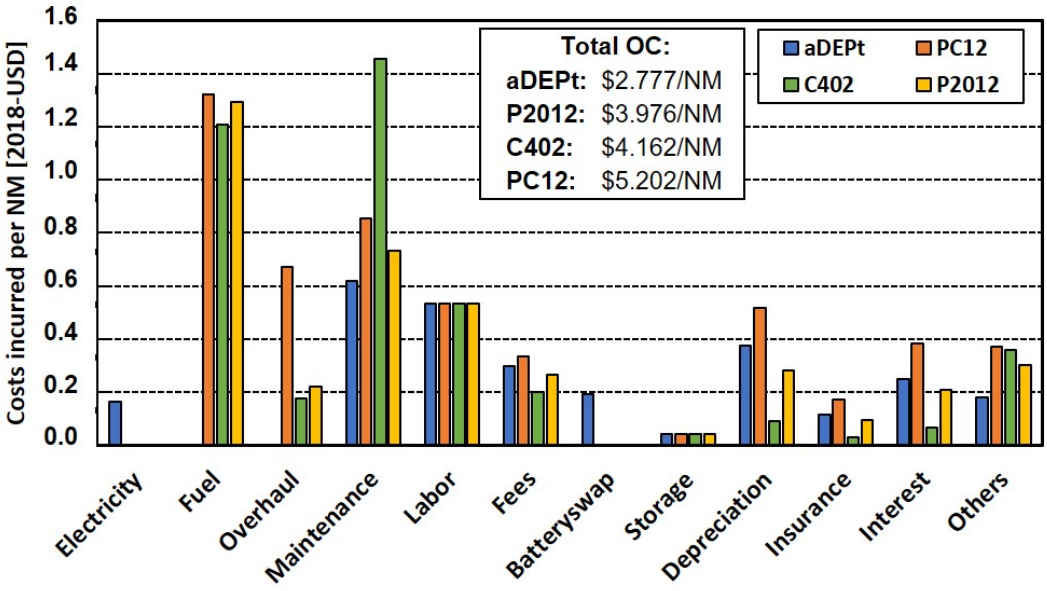

Figure 7.2: Operating cost estimates of the *aDEPt* and reference aircraft

Taking into account the purchase price, the *aDEPt* is therefore more profitable than PC12 from the outset. Amortization in relation to P2012 is achieved after one operating year. The Cessna 402 is no longer produced and is hence not considered here.

Total Life Cycle Costs

Disregarding the DC, the total LCC of one aircraft can be calculated from Equation 7.2. It should be noted that the LCC only consider real cash flows, therefore the depreciation costs (OC_{DP}) have to be deducted from the total OC.

$$LCC = \frac{DDC}{PR} + PC + t_{OP} * (OC - OC_{DP}) \tag{7.2}$$

An operating period (t_{OP}) of 20 years is assumed. The resulting LCC amount to **$23 206 142**. Of these, 89.5% are OC, 7.7% PC and 2.8% DDC.

7.2 Impact of Autonomy

In order to illustrate the influence of autonomous flights on costs, insurance and labor costs need to be examined. In accordance to section 5.2 a GP is needed out of safety reasons. It is assumed that on average one ground pilot can oversee five aircraft for the same cost rate of $40/h [24]. Furthermore, the GP will only monitor the aircraft for the duration of its block time. Additionally, it is assumed that insurance costs will initially rise for pilotless aircraft due to the risk aversion of insurance groups. However, it is expected that autonomous flying will reduce the risk of accidents, otherwise the technology will not be able to establish itself on the market. Therefore insurance costs for FAR Part 23 certified aircraft might actually decrease during the operating life of an aircraft. Yet, to give a conservative estimation, insurance costs for autonomous cargo missions are not changed compared to section 7.1. For a fully autonomous mission in a distant future the FAR Part 25 rates are applied, as the technology must already be well established on the market to ensure autonomous passenger transport.

Figure 7.3 illustrates how autonomy effects the costs related to the total operating time of 20 years. Since the *aDEPt* is already equipped for autonomous cargo operations when it is launched on the market, no change in DDC and PC can be observed. On the contrary OC and LCC decrease by 6.37% and 6.59%, respectively if an autonomous cargo mission is taken into account. This leads to OC of $2.600/NM ($315/flight, $0.289/ASM, $425/flighthour), making the *aDEPt* even more viable compared to its competitors. In case of fully autonomous operations, the OC and LCC decrease by 21.84% and 22.58%, respectively, leading to OC of $2.171/NM ($263/flight, $0.241/ASM, $355/flighthour).

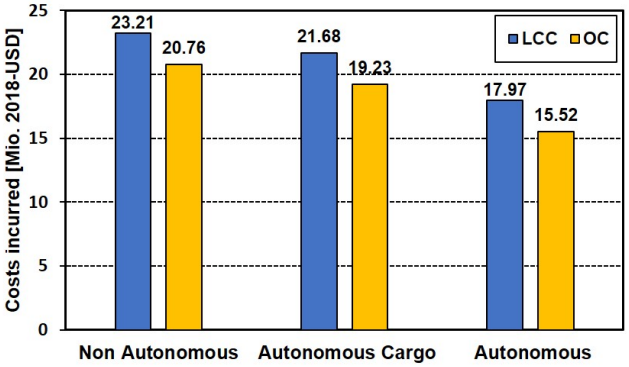

Figure 7.3: Impact of autonomy on costs

8 Conclusion

The *aDEPt* presents a versatile aircraft concept that offers an efficient and cost-effective transport model for connecting remote towns or small cities to larger central hubs in metropolitan areas. By combining a hybrid-electrical DEP approach with increased autonomy, the three biggest challenges of commuter airlines are addressed: high OC, lack of qualified pilots and demanding routes.

With its T/O and landing range of just under 160 m the *aDEPt* can land at almost every airport in the world and enables compatibility with future small airparks who might emerge in suburban areas. This is supported by the low noise level of 64.35 dB at the flyover point specified in procedure 24 CFR Part 36 Appendix G. In addition to the multi-redundant hybrid-electric DEP configuration, the dual cruise motor configuration, powertrain system architecture, and improved avionics further decrease error-proneness. Additionally the *aDEPt's* avionic configuration allows for autonomous operations, making it a sustainable aircraft for the future.

Through the sensible cabin conversion and loading concept, its electrical range of 125 NM at a maximum cruise speed of 250 kts, as well as the maximum range of 350 NM (within 99 min), the *aDEPt* provides numerous operational possibilities for any airline. In combination with the high W/S and the morphed TE the *aDEPt* further offers passengers a smooth, gust insensitive, flight feeling and at the same time increases its cruise performance significantly. This is especially evident in the high L/D of 23.9 at a cruise speed of 200 kts, which is a typical cruise speed for commuter aircraft.

The combination of its numerous key technologies ultimatly makes the *aDEPt* several times cheaper to operate than its direct competitors. In comparison with the Cessna 402, Pilatus PC12 and Tecnam P2012, initial calculations show savings in OC of 31.2%, 33.3% and 53.3%, respectively, when operated by one pilot. This advantage further increases to 34.6%, 37.5% and 50%, respectively, if cargo missions are flown autonomously and 45.4%, 47.3% and 58.3%, respectively, if all missions are flown autonomously.

Looking ahead to 2025 and beyond the *aDEPt* awaits emerging challenges and will contribute to connecting more people through air travel while enabling a more sustainable world.

Number	Name	Unit	Threshold	Goal	aDEPt	Reference
1	Max. Range	[NM]	200	500	**350**	3.2, 4.3
2	Alternate Airport	[NM]	50	100	**100**	3.2
3	T/O and Landing	[ft]	1000	250	**520**	4.1
4	Noise	[dB]	80	65	**64.35**	4.2
5	OC (1 pilot)	[2018-$/ASM]	-	-	**0.309**	7.1
6	OC (autonomous cargo)	[2018-$/ASM]	-	-	**0.289**	7.1
7	OC (fully autonomous)	[2018-$/ASM]	-	-	**0.241**	7.2

Table 8.1: Overview of requirements and degree of fulfillment

Bibliography

[1] Aminian, N. ; Romli, F.: Ergonomics assessment of current aircraft passenger seat design against Malaysian anthropometry data. In: *International Journal of Engineering & Technology* 7 (2018), No. 4.13, P. 18

[2] ARK Invest: *Supercharger: A Charge Could Cost Half the Price of Gas*. 2016. – URL `https://ark-invest.com/research/supercharger-cost-comparison#fn-6240-2`. – Date of access: 12.06.2019

[3] Arnhem, N. ; Sinnige, T. ; Stokkermans, T. C. ; Eitelberg, G. ; Veldhuis, L. L.: Aerodynamic Interaction Effects of Tip-Mounted Propellers Installed on the Horizontal Tailplane. In: *2018 AIAA Aerospace Sciences Meeting*. Reston, Virginia : American Institute of Aeronautics and Astronautics, 01082018. – ISBN 978-1-62410-524-1

[4] Bachrach, A. ; Winter, A. de ; He, R. ; Hemann, G. ; Prentice, S. ; Roy, N.: RANGE - robust autonomous navigation in GPS-denied environments. In: *2010 IEEE International Conference on Robotics and Automation*, IEEE, 03.05.2010 - 07.05.2010, P. 1096–1097. – ISBN 978-1-4244-5038-1

[5] Boeing: *Boeing 787: From the Ground Up*

[6] Borer, N. K. ; Patterson, M. D. ; Viken, J. K. ; Moore, M. D. ; Clarke, S. ; Redifer, M. E. ; Christie, R. J. ; Stoll, A. M. ; Dubois, A. ; Bevirt, J. ; Gibson, A. R. ; Foster, J. F. ; Osterkamp, P. G. ; American Institute of Aeronautics and Astronautics (Publ.): *Design and Performance of the NASA SCEPTOR Distributed Electric Propulsion Flight Demonstrator*

[7] Bray, R. S. ; National Aeronautics and Space Administration (Publ.): *A head-up display format for application to transport aircraft approach and landing*

[8] Cape Air: *Cessna 402C Limitations/Systems Review Guide*

[9] Coulsdon, Surrey: *IHS Jane's Aero-Engines*. IHS Global Limited, 2014. – ISBN 978-0-7106-3092-6

[10] DHL: *Versandkosten für Ihre Päckchen und Pakete*. 2019. – URL `https://www.dhl.de/de/privatkunden/preise.html`. – Date of access: 20.06.2019

[11] Diouf, B. ; Pode, R.: Potential of lithium-ion batteries in renewable energy. In: *Renewable Energy*. 2015, P. 375–380

[12] Drela, M. ; Youngren, H.: *XFOIL: Subsonic Airfoil Development System.* – URL `https://web.mit.edu/drela/Public/web/xfoil/`. – Date of access: 26.06.2019

[13] Eckl-Dorna, W. ; manager magazin (Publ.): *Boeing heizt Wettlauf um autonome Flugtaxis an.* – URL `https://www.manager-magazin.de/unternehmen/industrie/flugauto-boeing-heizt-wettlauf-um-autonome-lufttaxis-mit-testflug-an-a-1249824.html`. – Date of access: 22.06.2019

[14] FlexSys: *FLEXIBLY ENGINEERING THE "IMPOSSIBLE".* – URL `https://www.flxsys.com/aero`. – Date of access: 18.06.2019

[15] Gibson, J. S. ; National Aeronautics and Space Administration (Publ.): *NON-ENGINE AERODYNAMIC NOISE INVESTIGATION OF A LARGE AIRCRAFT*

[16] Grundhoff, S. ; FOCUS (Publ.): *Das heutige Elektroauto ist tot: Autobauer bereiten sich auf die "Post-Lithium-Ära" vor.* – URL `https://www.focus.de/auto/elektroauto/festkoerperbatterie-vor-dem-durchbruch-der-grosse-sprung-in-2025_id_9315733.html`. – Date of access: 22.06.2019

[17] Gudmundsson, S.: *General Aviation Aircraft Design: Applied Methods and Procedures.* Elsevier Inc., 2014

[18] Haines, R. F. ; Fischer, E., Prince, T. ; National Aeronautics and Space Administration (Publ.): *Head-Up Transition Behavior of Pilots With and Without Head-Up Display in Simulated Low-Visibility Approaches*

[19] Harish, A. ; Perron, C. ; Bavaro, D. ; Ahuja, J. ; Ozcan, M. ; Justin, C. Y. ; Briceno, S. I. ; German, B. J. ; Mavris, D.: Economics of Advanced Thin-Haul Concepts and Operations. In: *16th AIAA Aviation Technology, Integration, and Operations Conference.* Reston, Virginia : American Institute of Aeronautics and Astronautics, 06132016, P. 1. – ISBN 978-1-62410-440-4

[20] IOS: *Flat pallets for intercontinental materials handling – Principal dimensions and tolerances: Standard*

[21] Jansen, R. ; Bowman, C. ; Jankovsky, A.: Sizing Power Components of an Electrically Driven Tail Cone Thruster and a Range Extender. In: *16th AIAA Aviation Technology, Integration, and Operations Conference.* Reston, Virginia : American Institute of Aeronautics and Astronautics, 06132016. – ISBN 978-1-62410-440-4

[22] Kota, S. ; Osborn, R. P. ; Ervin, G. N.: *Mission Adaptive Compliant Wing - Design, Fabrication and Flight test*

[23] Kraft, A.: *Festkörperakku: Fraunhofer Institut entwickelt effizienteren Akku.* 2018. – URL `https://aiomag.de/`

festkoerperakku-fraunhofer-institut-entwickelt-effizienteren-akku-9003. – Date of access: 22.06.2019

[24] Kreimeier, M.: *Evaluation of On-Demand Air Mobility Concepts with Utilization of Electric Powered Small Aircraft*, RWTH Aachen, Dissertation, 2018

[25] Loh, R. ; Bian, Yi ; Roe, T.: UAVs in civil airspace: Safety requirements. In: *IEEE Aerospace and Electronic Systems Magazine* 24 (2009), No. 1, P. 5–17. – ISSN 0885-8985

[26] Marte, Jack F. ; Kurtz, Donald E. ; National Aeronautics and Space Administration (Publ.): *A Review of Aerodynamic Noise From Propellers, Rotors and Lift Fans*

[27] Metrass-Mendes, A. ; Neufville, R. ; Costa, A.: *Air Accessibility In Northern Canada; Prospects And Lessons For Remote Communities*

[28] Moormann, D.: *Flugdynamik;*. 2019

[29] National Aeronautics and Space Administration: *NASA Successfully Test Shape-Changing Wing for Next Generation Aviation*. 2015

[30] Norris, G. ; Aviation Week Network (Publ.): *Motor Mounting Marks Mileston For NASA's Electric X-plane*. 2018. – URL https://aviationweek.com/future-aerospace/motor-mounting-marks-milestone-nasa-s-electric-x-plane. – Date of access: 22.06.2019

[31] Nykvist, B. ; Nilsson, M.: Rapidly falling costs of battery packs for electric vehicles. In: *Nature Climate Change*. 2015, P. 329–332

[32] Patterson, Michael D. ; Borer, Nicholas K.: Approach Considerations in Aircraft with High-Lift Propeller Systems. In: *17th AIAA Aviation Technology, Integration, and Operations Conference*. Reston, Virginia : American Institute of Aeronautics and Astronautics, 06052017. – ISBN 978-1-62410-508-1

[33] Patterson M. D.: *Conceptual Design Of High Lift Propeller Systems For Small Electric Aicraft*, Georgia Institute of Technology, Dissertation, 2016

[34] Pilatus Aircraft Ltd: PC-12 NG Just The Facts. (2016)

[35] Porta, J. ; Saco-Ledo, G. ; Cabanas, M.: The ergonomics of airplane seats: The problem with economy class. In: *International Journal of Industrial Ergonomics* 69 (2019), P. 90–95

[36] Propfe, B. ; Redelbach, M. ; Santini, D. J. ; Friedrich, H. ; Mercedes, S.: Cost Analysis of Plug-in Hybrid Electrical Vehicles including Maintenance & Repair. In: *EVS26 International Battery, Hybrid and Fuel Cell Electric Vehicle Symposium*, 2012

[37] Purser, P. E. ; Campbell, J. P. ; American Institute of Aeronautics and Astronautics (Publ.): *Experimental Verification Of A Simplified Vee-Tail Theory And Analysis Of Available Data On Complete Models With Vee Tails*

[38] Raballand, G. ; Aldaz-Carroll, E.: How Do Differing Standards Increase Trade Costs? The Case of Palletts. In: *The World Bank* (2005), No. World Bank Policy Research Working Paper 3519

[39] Raymer, D. P.: *Aircraft Design: A Conceptual Approach*. Washington D.C. : American Institute of Aeronautics and Astronautics, 2006

[40] Rice, S. ; Kraemer, K. ; Winter, S. ; Mehta, R. ; Dunbar, V. ; Rosser, T. ; Moore, J.: Passengers from India and the United States Have Differential Opinions about Autonomous Auto-Pilots for Commercial Flights. In: *International Journal of Aviation, Aeronautics, and Aerospace* (2014)

[41] Rocky Mountain Power: *Industrial Price Comparison*. 2019. – URL `https://www.rockymountainpower.net/about/rar/ipc.html`. – Date of access: 12.06.2019

[42] Roy, S. ; Maheshwari, A. ; Crossley, W. A. ; DeLaurentis, D. A.: A Study on the Impact of Aircraft Technology on the Future of Regional Transportation Using Small Aircraft. In: *2018 Aviation Technology, Integration, and Operations Conference*. Reston, Virginia : American Institute of Aeronautics and Astronautics, 06252018, P. 13. – ISBN 978-1-62410-556-2

[43] Sea Air Transport & Service: *Was bedeutet der Begriff Volumengewicht/Chargeable Weight?* 2019. – URL `https://www.sats-logistics.com/glossar/volumengewicht-chargeable-weight/`. – Date of access: 12.06.2019

[44] Selfridge, R. ; Moffat, D. ; Reiss, J. D.: Physically Derived Sound Synthesis Model of a Propeller. In: *ACM* (2017)

[45] Settele, F. ; Knoll, A.: Untersuchung der Flugleistung eines Elektroflugzeuges mit einem neuartigen Elektromotor. In: *Deutscher Luft- und Raumfahrtkongress* (2015)

[46] Smith, J. C. ; Viken, J. K. ; Huerreiro, N. M. ; Dollyhigh, S. M. ; Fenbert, J. W. ; Hartmann, C. L. ; Kwa, T.-S. ; Moore, M. D.: Projected Demand and Potential Impacts to the National Airspace System of Autonomous, Electric, On-Demand Small Aircraft. In: *12th AIAA Aviation Technology, Integration, and Operations (ATIO) Conference and 14th AIAA/ISSMO Multidisciplinary Analysis and Optimization Conference*. Reston, Virigina : American Institute of Aeronautics and Astronautics, 09172012. – ISBN 978-1-60086-930-3

[47] Souppouris, A. ; The Verge (Publ.): *Morph: a Bold Seating Concept for Flexible Air Travel*. 2013. – URL `https://www.theverge.com/2013/11/13/5096636/morph-airplane-seating-concept-seymourpowell`. – Date of access: 13.11.2013

[48] Stoll, A. M. ; Mikic, G. V.: Design Studies Of Thin-Haul Commuter Aircraft with Distributed Electric Propulsion. In: *16th AIAA Aviation Technology, Integration, and Operations Conference*. Reston, Virginia : American Institute of Aeronautics and Astronautics, 06132016. – ISBN 978-1-62410-440-4

[49] Stoll, Alex M. ; Bevirt, JoeBen ; Moore, Mark D. ; Fredericks, William J. ; Borer, Nicholas K.: Drag Reduction Through Distributed Electric Propulsion. In: *14th AIAA Aviation Technology, Integration, and Operations Conference*. Reston, Virginia : American Institute of Aeronautics and Astronautics, 06162014. – ISBN 978-1-62410-282-0

[50] Stumpf, E.: *Flugzeugbau II ; Stabilität und Steuerbarkeit*. 2019

[51] TECNAM: P2012 TRAVELLER. (2017)

[52] Torenbeek, E.: *Advanced aircraft design: Conceptual design, analysis, and optimization of subsonic civil airplanes*. John Wiley & Sons Inc, 2013. – ISBN 9781118568088

[53] United Nations Department of Economic ; Social Affairs: World Urbanization Prospects, 2014 Revision. In: *US Air Force Wright Lab., Wright–Patterson AFB, OH, Rept. WL-TR-93-3082* (2014)

[54] Viken, S. A. ; Brooks, F. M. ; Johnson, S. C. ; American Institute of Aeronautics and Astronautics (Publ.): *Overview of the Small Aircraft Transportation System Project Four Enabling Operating Capabilities*

[55] Wei, F. ; Grubesic, T. H.: A Typology of Rural Airports in the United States: Evaluating Network Accessibility. In: Southern Regional Science Association (Publ.): *The Review of Regional Studies*, 2015

[56] Weintraub, Daniel J. ; Haines, Richard F. ; Randle, Robert J.: Head-Up Display (HUD) Utility, II: Runway to Hud Transitions Monitoring Eye Focus and Decision Times. In: *Proceedings of the Human Factors Society Annual Meeting* 29 (1985), No. 6, P. 615–619. – ISSN 0163-5182

[57] Wells, D. P. ; Horvath, B. L. ; McCullers, L. A.: *The Flight Optimization System Weights Estimation Method*

[58] Willert-Porada, M.: *Advances in Microwave and Radio Frequency Processing*. Berlin, Heidelberg : Springer Berlin Heidelberg, 2006. – ISBN 978-3-540-43252-4

[59] Wolf, D. ; Markham, L.: *Commuter Airline Persepctive: On-Demand Mobility and Follow Up Workshop*. 08.03.2016

[60] Wolf, D. A. ; House Commitee in Transportation and Infrastrucure Subcommittee on Aviation (Publ.): *Air Service to Small and Rural Communities*

[61] Wolfgang Kempkens: *Nasa experimentiert mit flexiblen Hinterkanten*. – URL `https://www.ingenieur.de/technik/fachbereiche/raumfahrt/dehnbare-huelle-laerm-wirbel-an-tragflaechen-senken/`. – Date of access: 18.06.2019

A Appendix

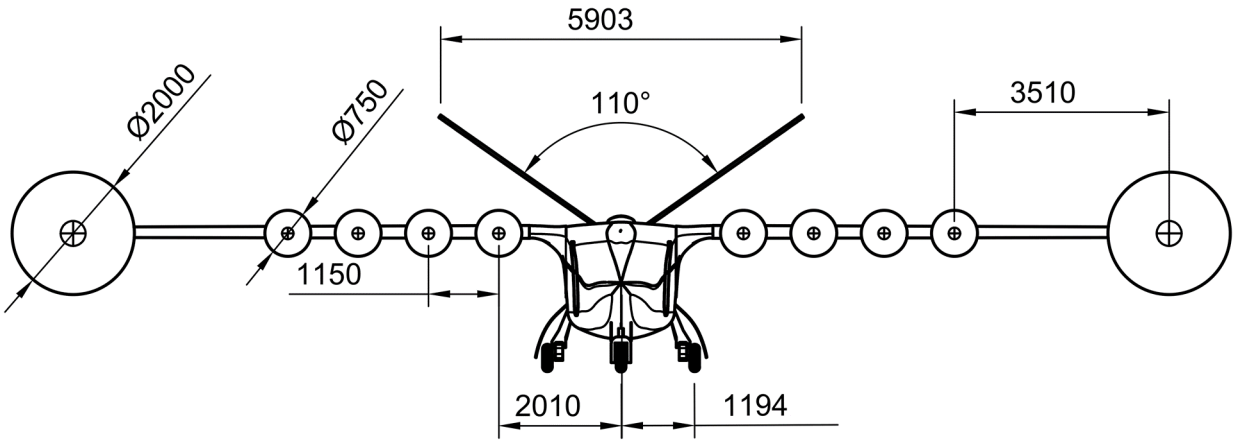

Figure A.1: Front view of the *aDEPt*

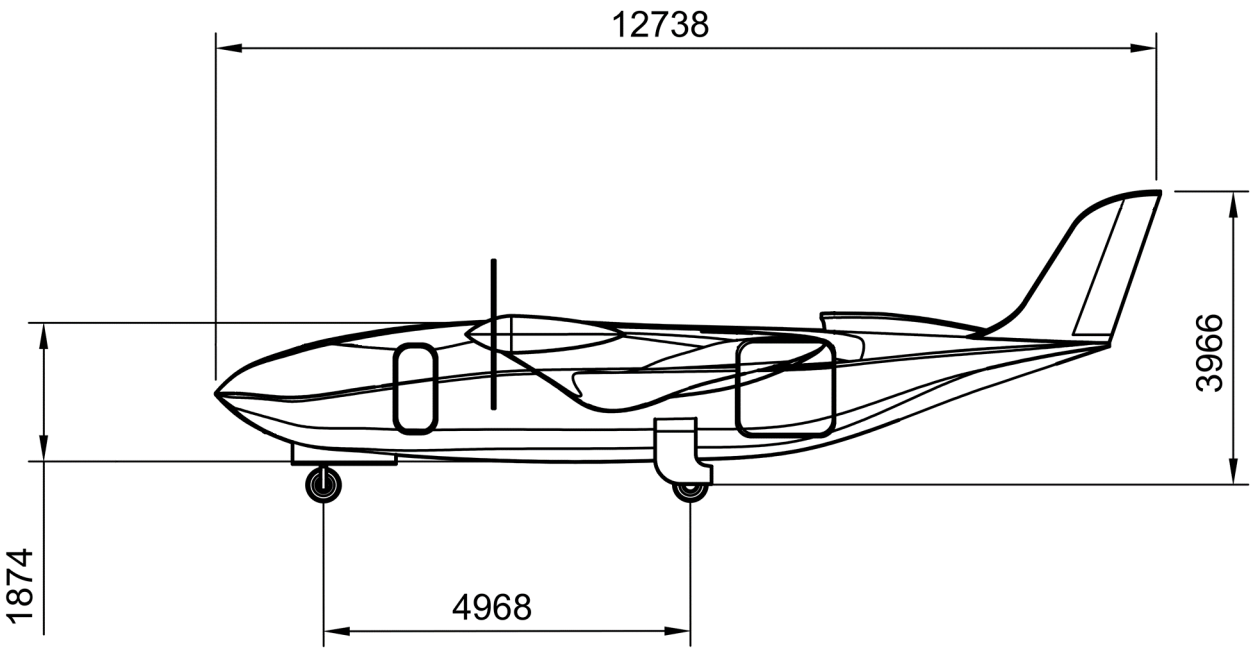

Figure A.2: Side view of the *aDEPt*

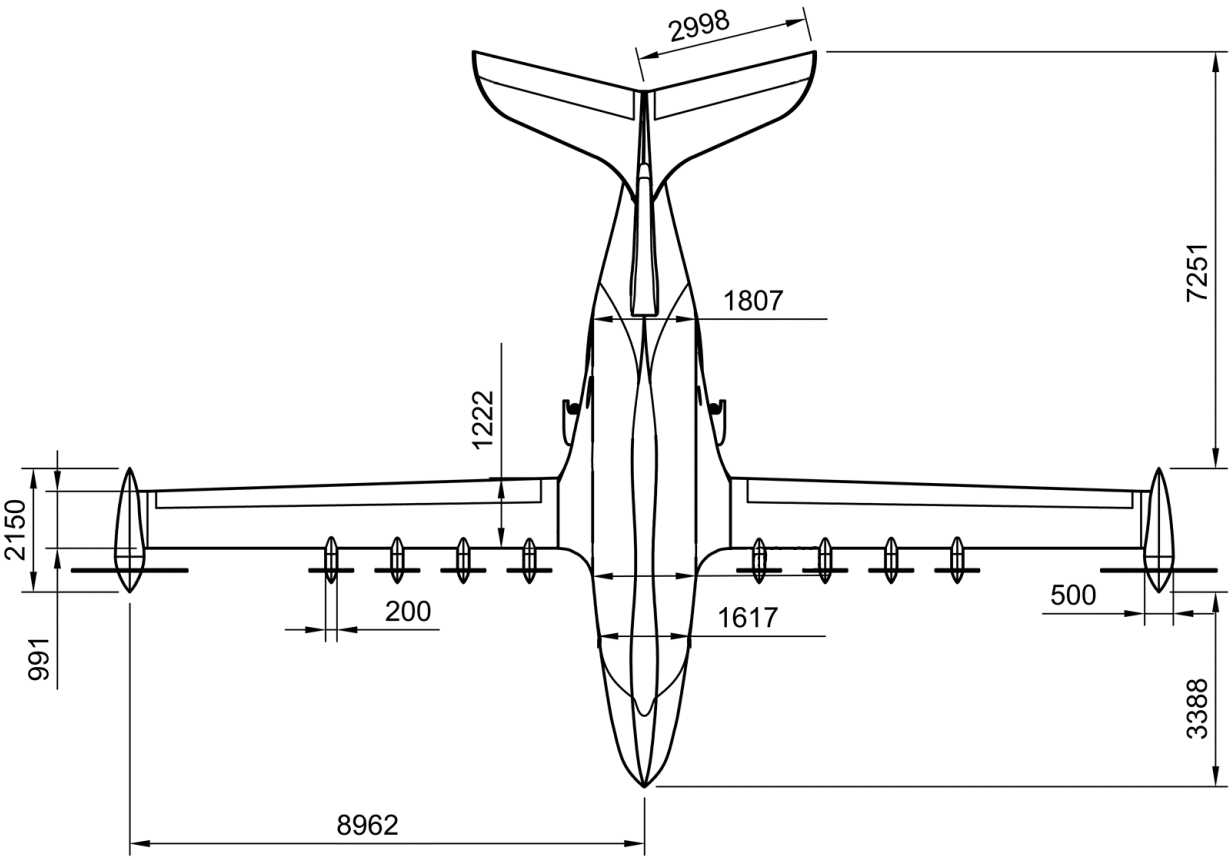

Figure A.3: Top view of the *aDEPt*

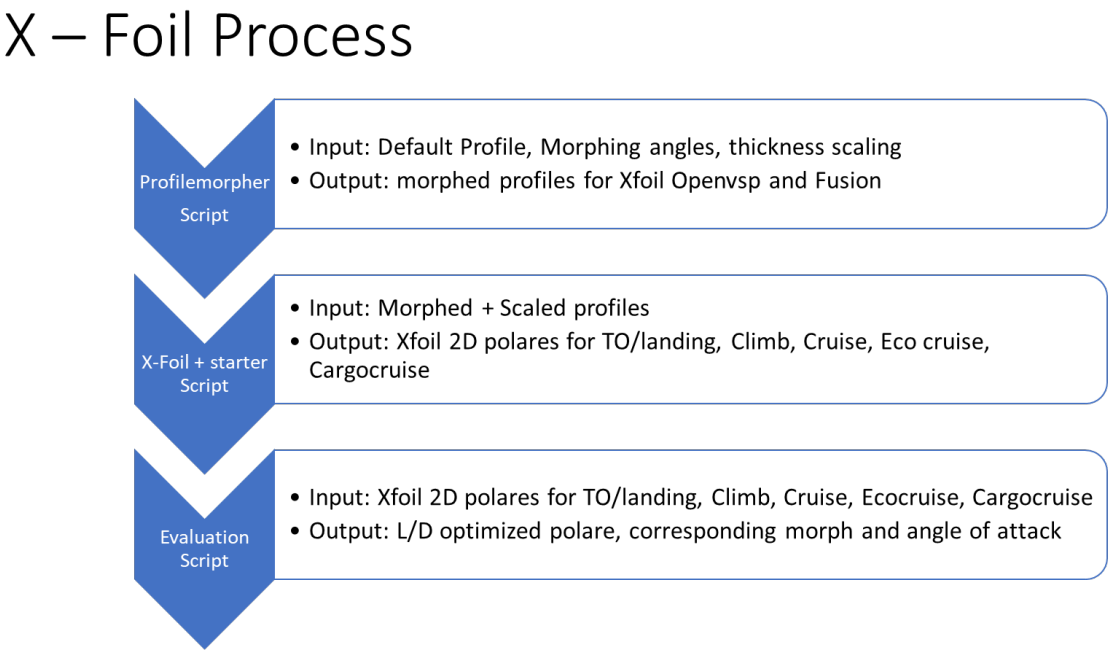

Figure A.4: Morphing wing calculation process overview

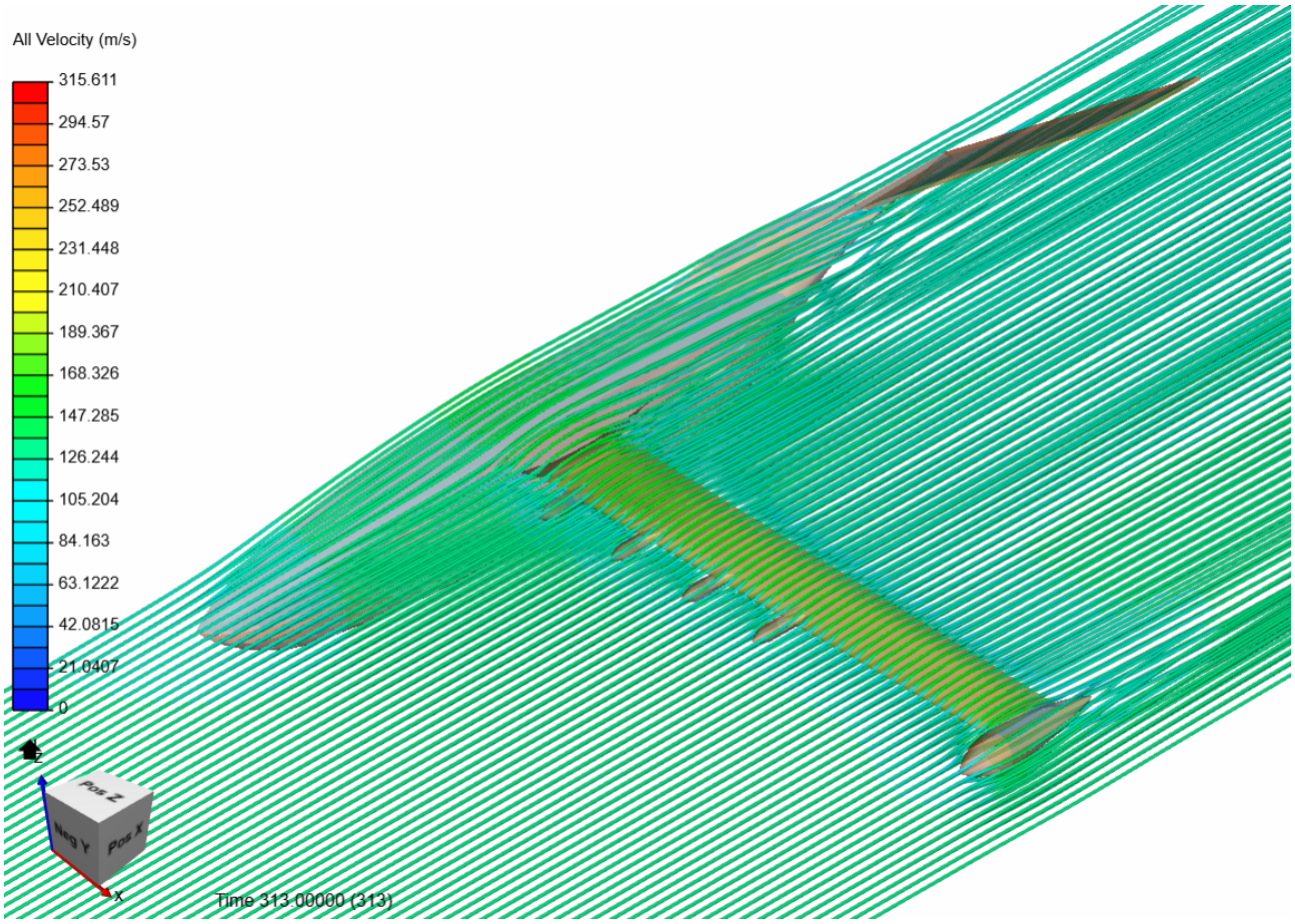

Figure A.5: Streamlines around the aircraft

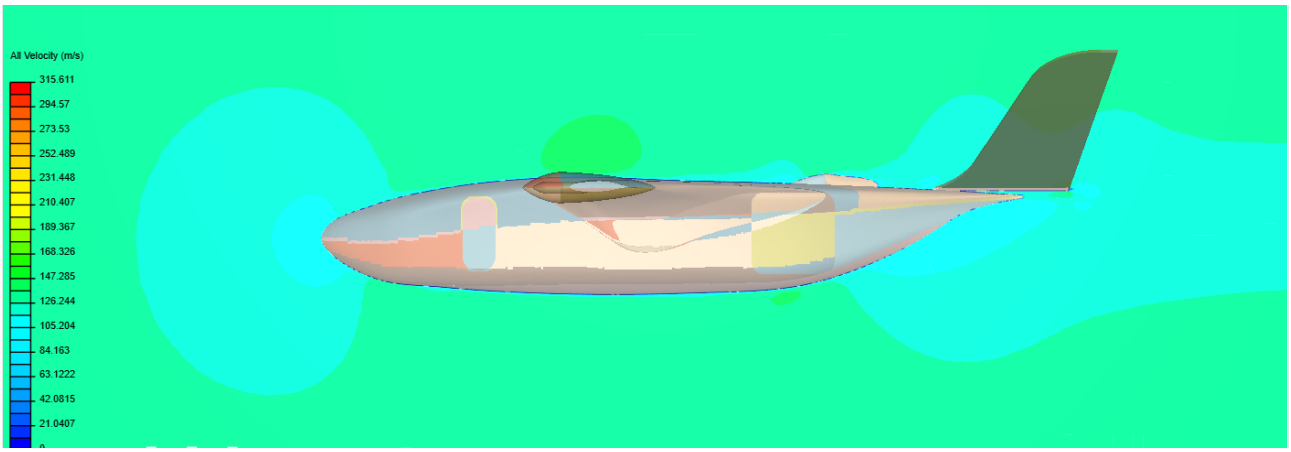

Figure A.6: Velocity distribution around the fuselage, 20cm off center

Figure A.7: View over the left aft of aDEPt

Figure A.8: View on the front left of aDEPt